University of Stavanger

**Faculty of Science and Technology**

# MASTER'S THESIS

| | |
|---|---|
| Study program/ Specialization:<br><br>**M. Sc. Petroleum Engineering / Production** | Spring semester, 2014<br>**Open access** |
| Writer:<br>**Antonio Jesus Heredia Garate** | 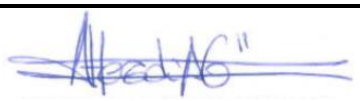 <br>(Writer's signature) |
| Faculty supervisor:<br>**Prof. Steinar Evje – University of Stavanger**<br>Co-supervisor:<br>**Prof. Pål Andersen – University of Stavanger**<br>External supervisor(s):<br>**None** | |
| Thesis title:<br><br>**Study of a Model for Spontaneous Imbibition as a Mechanism for Oil Recovery in Naturally Fractured Reservoirs** | |
| Credits (ECTS): **30 ECTS** | |
| Key words:<br>Spontaneous Imbibition.<br>Naturally Fractured Reservoirs.<br>Linear Transfer Function.<br>Fracture Matrix Geometry.<br>Waterflooding.<br>Transfer Rate Constant. | Pages: 68<br><br>+ enclosure: 12<br><br>Stavanger, June 2014<br>Date/year |

Front page for master thesis
Faculty of Science and Technology
Decision made by the Dean October 30th 2009

**Abstract**

One of the principal recovery mechanisms in Naturally Fractured Reservoirs (NFRs) is spontaneous imbibition. Understanding the parameters affecting spontaneous imbibition is the first step to achieve optimum oil recovery in NFRs. The effects of changing flow rate of injected water, wettability, rock properties, capillary pressure, fracture width and fluids viscosities are studied using a simplified model. Furthermore, a linear transfer function, used to model spontaneous imbibition, is evaluated.

A numerical model developed at the University of Stavanger is used to describe fracture matrix flow. Transport due to advection takes place in the fracture and capillary forces influence flow in the direction perpendicular to the fracture. Two dimensionless parameters describing fracture matrix flow are studied: $\alpha = \frac{\tau^f}{\tau^{c,m}}$ which is the ratio of the time for flow in the fracture to the time for flow in the matrix and $\beta = \frac{V^M}{V^f}$ which is the ratio of matrix pore volumes to fracture pore volumes.

After studying the dimensionless parameters, the model is modified by introducing a linear transfer function of the form $T = B\phi^M(S_{eq} - S_w^M)$ to account for the mass exchange between fracture and matrix. Numerical simulations are used to compare the modified and the original model. Physical parameters affecting the rate constant $B$ are investigated.

As a result, it was found that when waterflooding takes place, a preferentially water-wet (PWW) system produces significantly more oil than a preferentially oil wet (POW) system.

Varying the dimensionless parameters respect to a base case, the following observations were made. When $\alpha$ increases at constant $\beta$, water imbibes deep in the matrix improving oil recovery. On the contrary when $\alpha$ decreases, poor oil recovery is observed. When increasing $\beta$ at constant $\alpha$, the water injection rate is reduced, improving oil recovery. When increasing $\beta$ and decreasing $\alpha$ water takes more time to travel in the fracture, hence there is more time for imbibition to occur, which improves oil recovery.

When the viscosity ratio is low ($\mu_w/\mu_o = 1/5$), more water imbibes in the matrix compared to the base case ($\mu_w/\mu_o = 1$). Reducing the water viscosity increases oil recovery by spontaneous imbibition.

The linear transfer function evaluated can reproduce the oil recovery curve produced by the original model. However, this transfer function cannot reproduce the linear behaviour of the recovery curve before breakthrough. Regarding the rate constant $B$, the following relation was observed $B \propto \frac{K^M}{\phi^M}$. Where $K^M$ is the matrix absolute permeability and $\phi^M$ is the porosity.

**Acknowledgements**

I would like to express my deepest gratitude to my faculty supervisors Steinar Evje and Pål Andersen for their excellent guidance while writing this master thesis. Without their previous work this thesis would not have been possible.

I would like to express my appreciation to my parents Rogelio and Irene for being an example of hard work and dedication. To my brothers Roger, Ariel, Rogelio and my sister Marcela for their support and encouragement during my studies.

I would like to thank my fellow students and friends, that I met throughout my studies, for giving me their friendship.

# Contents

# List of Figures

# List of Tables

# Chapter 1

# Introduction

## 1.1 Background

Naturally fractured reservoirs (NFR) represent over 20% of the world's oil reserves [21]. Examples of prolific hydrocarbon reservoirs include the Monterrey Shales in California, the West Texas carbonates, the Asmari Limestone in Iran and the North Sea Chalks. These fields generally have active aquifers associated with them, and most will eventually go through a process of secondary recovery by waterflooding [20]. Planing waterflooding in a NFR is additionally challenging because of the complexity of the fractures' geometry. Interaction between rock, oil and water in a NFR is complex. Understanding the fluid flow mechanisms is the first step to achieve optimum oil recovery.

The Ekofisk field, in the North Sea, is an example of waterflooding of a NFR. This field produces from naturally fractured chalk in the Ekofisk and Tor Formations of Early Paleocene and Late Cretaceous ages. The reservoir rocks have high porosity, but low permeability. Ekofisk was originally developed by pressure depletion and had an expected recovery factor of 17 per cent. Since then, limited gas injection and comprehensive water injection have contributed to a substantial increase in oil recovery. Large scale water injection started in 1987, and in subsequent years the water injection area has been extended in several phases. Experience has proven that water displacement of the oil is more effective than anticipated, and the expected recovery factor for Ekofisk is now approximately 50 per cent [8].

Fractured porous media are usually divided into matrix and fracture systems. The matrix system contains most of the fluid storage, but fluid movement is slow [20]. Fractures contain little fluid relative to the matrix, but fluids flow more easily.

Production from NFR can be associated with various physical mechanisms. Oil expansion, spontaneous imbibition, gravity drainage, diffusion and viscous

displacement. One of the principal recovery mechanisms in NFRs is spontaneous imbibition, controlled by capillary forces, where water enters the matrix from the fractures, displacing oil [18]. Imbibition is defined as the displacement of one fluid by another immiscible fluid. In two-phase flow in porous media, spontaneous imbibition occurs when a wetting fluid displaces a non-wetting fluid, contrary to drainage where the non-wetting phase displaces the wetting fluid.

To increase oil recovery in NFRs by means of waterflooding, it is important to understand the physical interactions between the rock, oil and water. Intuitively, we expect injected water to flow primarily through low flow resistance fractures rather than the high flow resistance matrix when capillary imbibition forces are weak. Thus, capillary forces must be relatively strong if water injection in fractured systems is going to be successful.

The present work aims to improve understanding of spontaneous imbibition in the process of waterfooding a NFR. For this purpose, the Study of a Model for Spontaneous Imbibition as a Mechanism for Oil Recovery in Naturally Fractured Reservoirs is presented. With the knowledge gained from this work increased understanding of different parameters affecting oil recovery by spontaneous imbibition in NFR will be achieved.

## 1.2 Motivation

Developing a Study of a Model for Spontaneous Imbibition as a Mechanism for Oil Recovery in Naturally Fractured Reservoirs, will provide understanding of the physical principles behind waterflooding a NFR. The parameters affecting spontaneous imbibition will be determined and described qualitatively. The role of flow rate of injected water, wettability, properties of the rock, capillary pressure and others will be studied. Furthermore, a linear transfer function used in streamline reservoir simulators will be evaluated and analysed.

A better understanding of the physical principles behind water flooding of a NFR, will improve waterflooding planning and performance. Better waterflood performance will increase the amount of oil produced from the reservoir. Positive economical repercussions will come attached to improved waterflood performance.

In this work, a model for oil displacement by water is studied. This model has been developed in the University of Stavanger (UIS) and is taken from [19]. The model is derived from the transport equations for incompressible, immiscible oil-water flow in porous rocks. The model provides insight into the role played by parameters like saturation functions, injection rate, volume of fractures versus volume of matrix, different viscosity relations, and strength of capillary forces versus injection rate.

## 1.3 Objectives

This work investigates how water displaces oil in a fracture-matrix geometry. A linear fracture symmetrically surrounded by porous matrix is considered. When water is injected, it displaces oil from the fracture towards the producing well but at the same time water imbibes in the matrix blocks and displaces oil towards the fracture.

The main objective of this work is to understand the factors affecting spontaneous imbibition by the use of a 1D+1D model developed at the University of Stavanger. The model uses the transport equations for oil and water in porous rocks together with Darcy equation to generate a system of partial differential equations describing the change in storage of water in the rock, the model considers the effect of advective displacement and capillary diffusion. The model is written for a 2D geometry. The equations are scaled and the system is solved using an operator splitting approach. A discrete scheme is generated to solve the equations numerically.

To achieve this objective the following secondary objectives are established:

1. Describe qualitatively the role of saturation curves of the porous rock.
2. Describe the role of the dimensionless parameters described in the 1D+1D model.
3. Identify the influence of the viscosity ratio on oil recovery.
4. Test a Linear Transfer Function when implemented in the 1D+1D model.

The approach that has been taken here, provides with qualitative description of oil displacement by water in a fracture matrix geometry.

## 1.4 Outline

Chapter one "Introduction" is a section describing the framework of the study. It introduces the motivation behind the investigation within the context of an important NFR in the North Sea, and sketches the motivation of the study and its objectives. At last it describes the structure of the present written work.

Chapter two "Literature Review" begins by introducing the most common approaches used in modelling of NFRs. Then it presents the concept of transfer function, taking a close look at the deduction of a linear transfer function. Important concepts like wettability and capillary pressure are discussed. Finally, an example of how scaling is used to simplify mathematical problems is presented.

Chapter three − "Model description" presents the transport equations for incompressible flow of oil and water. The fracture-matrix geometry used in this work is presented. The 1D+1D model is scaled using dimensionless parameters and $\alpha$ and $\beta$ quantities are introduced. The initial and boundary conditions are established. The relative permeability and the capillary pressure curves are described. At the end of the chapter a modification of the 1D+1D model using a linear transfer function is introduced.

Chapter four − "Numerical Investigations" presents the input parameters used in the 1D+1D model. The impact of the system wettability is investigated. The importance of $\alpha$, $\beta$ and viscosity ratio $\mu_w/\mu_o$ is studied.

Chapter five − "Linear Transfer Function Testing" presents a study of a transfer function of the form $T = B\phi^M(S_{eq} - S^M)$. The main focus is to understand the physical parameters modifying the rate constant $B$. The influence of system wettability, grid size ($n_x$ and $n_y$), matrix permeability ($K^M$) and porosity ($\phi^M$) are evaluated.

Chapter six − "Discussion and Conclusions" summarizes and points out important aspects presented in the previous chapters regarding the 1D+1D model and the linear transfer function. A review of the goals of this work is contrasted with the results of the investigation. At the end of the chapter, conclusions of this work are stated.

Appendix A − "Matrix Saturation and Capillary Pressure Plots for Preferentially Water-Wet system" presents a comparison of saturations and capillary pressures inside the matrix in a preferentially water wet (PWW) system. These were calculated using the 1D+1D and the linear transfer function models.

Appendix B − "Matrix Saturation and Capillary Pressure Plots for Preferentially Oil Wet system" presents a comparison of saturations and capillary pressures inside the matrix in a preferentially oil wet (POW) system. These were calculated using the 1D+1D and the linear transfer function models.

Appendix C − "Influence of grid size on Rate constant $B$" presents various plots showing that the grid size used in the calculations have an impact on the rate constant $B$.

Appendix D − "Numerical discretization of the linear transfer function" presents the algebraic equations used to calculate the solutions of the linear transfer function.

Appendix E − "Nomenclature" presents the variables, abbreviations, subscripts and superscripts used throughout this work.

# Chapter 2

# Literature review

This chapter describes relevant concepts for modelling oil water flow in a fracture matrix geometry.

## 2.1 Fracture-matrix flow

In NFRs, fractures provide the main path for fluid flow from the reservoir, usually the oil from the matrix blocks flows into the fracture space, and the fractures carry the oil to the wellbore [15].

Two approaches are used in order to model NFRs. The first is a dual porosity approach and the second is a discrete fracture/discrete matrix approach. Both are discussed in the following:

The dual porosity approach considers the reservoir as containing two interacting media: the fractures that carry the flow and the matrix that stores the oil. The geometry of the fracture and matrix is not represented in detail, instead, it is replaced by a regularized (grid block) representation of the field [10]. In this model one porosity is associated with the matrix blocks and the other with the fractures. In a field scale reservoir simulation using the dual-porosity approach, fluid exchange between fracture and matrix is described by a single transfer function [12]. In Fig.2.1 taken from [15], it is possible to see an schematic view of a fracture network together with the matrix blocks. If the matrix blocks are linked only through the fracture system, this could be regarded as a dual porosity single permeability system, since fluid flow through the reservoir takes place only in the fracture network with the matrix blocks acting as sources. If there is the possibility of flow directly between neighbour matrix blocks, this is conventionally considered to be a dual porosity dual permeability system [23].

Significant work has been made to develop appropriate transfer functions to account the mass exchange from the matrix to the fracture network (A discussion

on transfer functions is presented in Section 2.2).

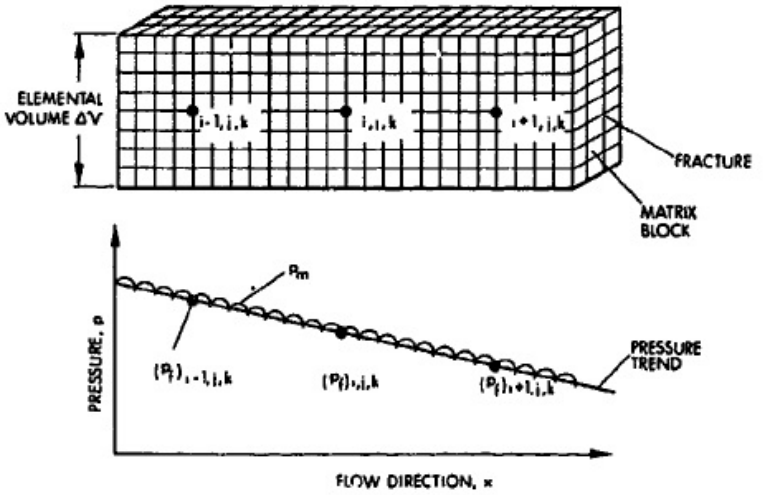


Figure 2.1: Idealization of flow and elemental reservoir volumes containing matrix blocks in a naturally fractured reservoir according to "Dual Porosity Model"

On the other hand, the discrete fracture/discrete matrix (DFDM) approach describes both the fracture and matrix with an explicit grid. This method is the most physically realistic and computationally accurate way to model flow in fractured media [10]. Capturing displacement in a geologically realistic fracture network requires a finely resolved grid and intricate indirect discretization approaches [10].

In this work a simplified 1D+1D model is used. This model describes displacement of oil by water in a single fracture surrounded by a matrix section. This model is transparent and considers that oil is displaced by advection inside the fracture and by capillary forces in the matrix [19]. Advection transport in the matrix and gravity are neglected.

## 2.2 Dual porosity approach and transfer functions

As mentioned in the previous section, when using the "Dual porosity" approach to simulate flow in NFRs, the fracture and matrix systems are separated into different continua, each with its own set of properties characteristic to the matrix and fracture systems. Matrix-fracture mass transfer is described through a "Transfer Function" [3]. With this definition, the formulation for a dual porosity model would be very similar to a conventional single porosity model, except for the presence of the tranfer function [22]. This transfer function is the heart of the dual porosity model because it controls performance of a NFR. The concept of a transfer function from a simulation point of view is presented in Figure 2.2 taken from [22].

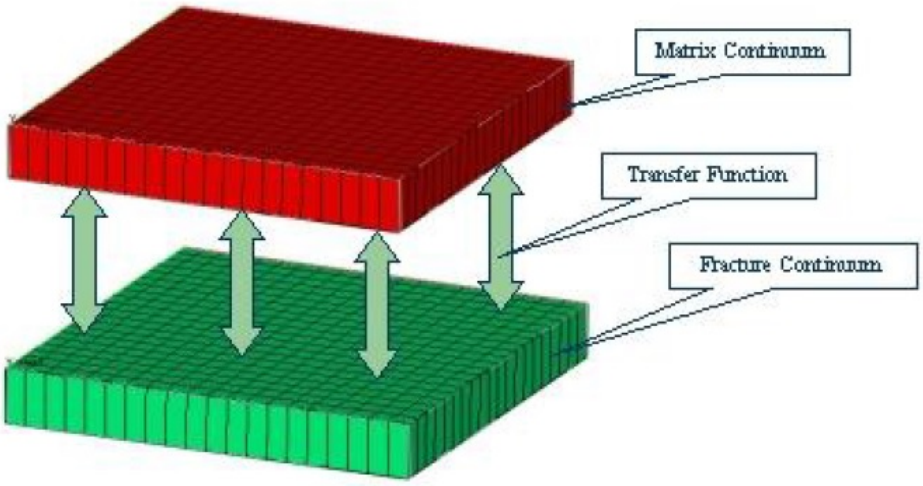


Figure 2.2: Tranfer function schematic

The equations describing the "Dual Porosity" approach for two phase flow are given by the following equations for the fracture and the matrix respectively:

$$\partial_t(\phi^f S) + \nabla(\phi V_t f_w^f(S) + K^f g[\lambda_o^f f_w^f](S)\Delta\rho\nabla z = -T \tag{2.1}$$

$$\partial_t(\phi^M S) = T \tag{2.2}$$

It can be seen from Eq. 2.1 and Eq.2.2, that the interaction between fracture and matrix is governed by the transfer function T. The transfer functions generally used assume that the mechanism governing fracture matrix flow is fluid

expansion and neglect additional mechanisms like imbibition and gravity segregation. Also, block averaged values of potential, saturation, capillary pressure and relative permeabilities are used in the transfer functions.

Two forms of transfer functions are presented in the following. The purpose of these functions is to model capillary-controlled counter current imbibition between matrix and fracture.

### 2.2.1 Linear transfer function

Many experiments have studied spontaneous imbibition, where water-wet cores have been surrounded by water, and oil recovery has been recorded [17]. Oil recovery can be matched by a simple exponential function of time. The following expression is suggested to match oil recovery.

$$R = R_\infty(1 - e^{-Bt}) \tag{2.3}$$

Where $R_\infty$ is the ultimate recovery, $R$ is the oil recovery, $B$ is a rate constant in $1/s$ and $t$ is the time in $s$. According to [7], the rate constant B is defined by:

$$B = 3\sqrt{\frac{K^M}{\phi^M}}\frac{\sigma}{L_c^2}\frac{J'\lambda_o\lambda_w}{\lambda_o + \lambda_w}\mid_{S_w^M = S_{eq}} \tag{2.4}$$

Where $K^M$ is the matrix permeability given in $m^2$, $\phi^M$ is the matrix permeability, $J'$ is the derivative of the $J$ function (See Section 2.7), $\lambda_i$ is the mobility of phase $i$ ($o$=oil, $w$=water) , $S_{eq}$ is the saturation at which imbibition stops, $\sigma$ is the interfacial tension between oil and water given in $N/m$ and $L_c$ is an effective length given in $m$, which is calculated with the formula:

$$L_c^2 = \frac{V}{\sum_{i=1}^{n}\frac{A_i}{l_i}} \tag{2.5}$$

Where $V$ is the matrix block volume in $m^3$, $A_i$ is the area open to flow in the $i^{th}$ direction given in $m^2$ and $l_i$ is the distance from the open surface to a no flow boundary.

If it is not possible to calculate the mobilities at the equilibrium saturation $S_{eq}$, $B$ constant may be calculated by a relation suggested in [26]:

$$B = b\sqrt{\frac{K^M}{\phi^M}}\frac{\sigma}{L_c^2\sqrt{\mu_o\mu_w}} \tag{2.6}$$

Where $b$ depends on the reservoir wettability and varies from 0.05 for strongly water-wet systems to $10^{-5}$ and lower for mixed wet systems. Matrix permeability $K^M$ is given in $m^2$, interfacial tension $\sigma$ is given in $N/m$ and viscosity $\mu_i$ in $Pa.S$

If $S_w^M$ is the average water saturation in the matrix, then the ratio of recovery and ultimate recovery is given by:

$$\frac{R}{R_\infty} = \frac{S_w^M - S_{wi}^M}{S_{eq} - S_{wi}^M} \tag{2.7}$$

Where $S_{wi}^M$ is the initial water saturation in the matrix. Thus:

$$S_w^M = S_{wi}^M + (S_{eq} - S_{wi}^M)(1 - \exp^{-Bt}) \tag{2.8}$$

From Eq. 2.8:

$$\phi^M \frac{\partial S_w^M}{\partial t} = T = B\phi^M (S_{eq} - S_{wi}^M) \tag{2.9}$$

It is possible to write the transfer function as:

$$\begin{aligned} T_1 &= B\phi^M (S_{eq} - S_w^M) \qquad S_w^f > 0 \\ &= 0 \qquad\qquad\qquad\qquad S_w^f = 0 \end{aligned} \tag{2.10}$$

Where the rate constant $B$ is defined by Eq. 2.6 [6]. Note that the transfer function is a linear function of the matrix saturation. This relations will be referred as the linear transfer function in this work.

This function considers the imbibition potential $\Delta S = (S_{eq} - S_w^M)$ as the driving force generating mass transfer between the matrix and fracture.

### 2.2.2 Conventional transfer function

In grid-based dual porosity formulation, transfer rates for both oil and water are defined using a Darcy type expression [13]:

$$T = T_w = FK^M \lambda_w^f (p_w^f - p_w^M) \tag{2.11}$$

$$T_o = FK^M \lambda_o^f (p_o^f - p_o^M) \tag{2.12}$$

Where F is the shape with the dimensions of $1/length^2$ which represents the inverse of the fracture spacing squared, $p_w^f$ is the pressure of the water phase in the fracture, $p_w^M$ is the pressure of the water phase in the matrix, $p_o^f$ is the pressure of the oil phase in the fracture, $p_o^M$ is the pressure of the oil phase in the matrix. Since there is no viscous mediated flow in the stagnant regions the capillary pressure is

given by, $p_c^M = p_o^M - p_w^M$. For incompressible flow $T_o + T_w = 0$. If it is assumed that the capillary pressure in the matrix is much higher than in the fracture ($p_o^f = p_w^f$), it is possible to derive the conventional transfer function [6]:

$$T_2 = FK^M \frac{\lambda_w^f \lambda_o^f}{\lambda_w^f + \lambda_o^f} p_c^M \tag{2.13}$$

## 2.3 Rock wettability

Rock wettability in a multiphase fluid system is the tendency of either the water phase or the oil phase to maintain contact with the rock surface. Thus, the surface of a water-wet rock, preferentially maintains contact with water, while the surface of an oil-wet rock will preferentially maintain contact with oil.

The most common method of determining rock wettability is by measurement of the contact angle $\theta$ between the rock surface and the fluid system as shown in Fig. 2.3 reproduced from [25]. The contact angle $\theta$ at the surface can range from 0 to 180°. Generally, when $\theta$ is between 0 to 75°, the system is defined as water-wet. When $\theta$ is between 105 to 180° the system is defined as oil-wet. In the middle range of contact angles, a system is neutrally or intermediately wet [1].

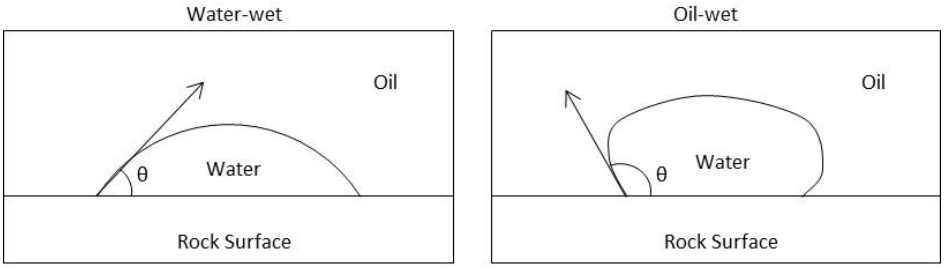


Figure 2.3: Contact angle describing system wettability

The oil composition affects the wettability of the rock. The wetting state of reservoir rock is affected by the presence of polar compounds such as asphaltenes, film forming components, and high molecular weight paraffins. Other factors that may affect rock wettability include type of minerals present in the rock, the reservoir rock type (quartz, silica, calcite, etc), and the salinity of the connate water [11].

## 2.4 Waterflooding and wettability

In this section, the importance of wettability on waterflood is described.

In a strongly water-wet rock at initial water saturation. The wetting phase, will occupy the small pores and form a thin film over all the rock surfaces [9].

Oil, the non wetting phase, will occupy the center of the larger pores. Any oil placed in the small pores would be displaced into the center of the large pores by spontaneous water imbibition [2].

During a waterflood of a water-wet system, water moves through the porous medium in a fairly uniform front [5]. In the zone where oil and water are flowing, a portion of the oil exists in continuous channels with some dead end branches. Figure2.4 a) taken from [24] shows water displacing oil from a water-wet pore. Water will advance through the walls of the pore, displacing oil in front of it. At some point, the neck connecting the oil in the pore with the remaining oil will become unstable and snap off, leaving a spherical oil globule trapped in the center of the pore. After the water front passes, almost all the remaining oil is immobile. Because of such immobility in this water-wet case, there is little or no production of oil after water breakthrough [4].

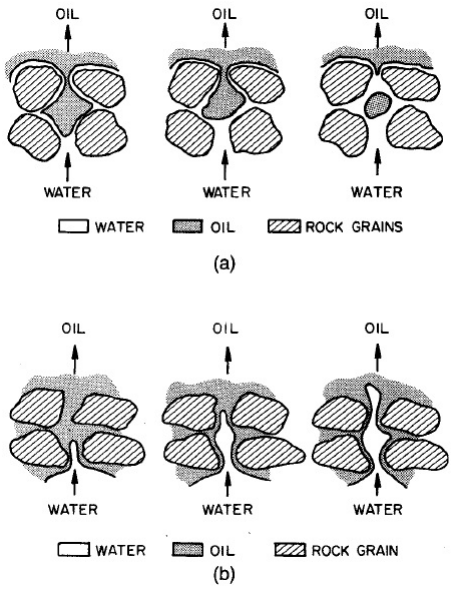


Figure 2.4: Water displacing oil from a pore during waterflood:
a) strongly water-wet system, b) strongly oil-wet system

In a strongly oil-wet rock, the rock is preferentially in contact with the oil, and the location of the two fluids is reversed from the water-wet case. Oil will generally be found in the small pores and as a thin film on the rock surfaces, while water will be located in the center of the larger pores.

During a waterflood in a strongly oil-wet rock, oil displacement is less efficient than one in a water-wet rock. When the waterflood starts, the water will form continuous channels or fingers through the centers of the larger pores, pushing oil in front of it, as shown in Figure 2.4 b). Oil is left in the smaller crevices

and pores. As water injection continues, water invades the smaller pores to form additional continuous channels, and the water oil ratio (WOR) of the produced fluids gradually increases [2].

## 2.5 Relative permeability curves in strongly wetted systems

Relative permeability curves measured on strongly water-wet and strongly oil-wet systems are presented in Fig. 2.5 taken from [14]. The plot shows relative permeability in water-wet and oil-wet systems. The relative permeability is measured as percent of the total permeability. These measurements were taken in a core composed of sintered aluminium oxide and fluids were brine and heptane. It can be noted form Fig. 2.5 that the water relative permeability is higher for the oil-wet system than the water-wet system. This happens because the wetting fluid travels through the smaller pores and the non-wetting fluid travels through the larger pores [2]. Regarding Fig. 2.5, at residual oil saturation, the water relative permeability is about 80% for oil-wet system and 40%for the water-wet system. The crossover point, where the water and oil relative permeabilities are equal, occurs at water saturation 35% PV for oil-wet core and 65% PV for the water-wet one. This observations agree with the rules of thumb presented in Table 2.1 [5].

Table 2.1: Craig's Rules of Thumb for Determining Wettability

| | Water-Wet | Oil-Wet |
|---|---|---|
| Residual Water Saturation | Usually grater than 20 to 25% PV | Generally less than 15% PV |
| Saturation at which oil and water relative permeabilities are equal | Greater than 50% water saturation | Less than 50% water saturation |
| Relative permeability to water at the maximum water saturation; based on the effective oil permeability at reservoir residual water saturation. | Generally less than 30%. | Greater than 50% and approaching 100% |

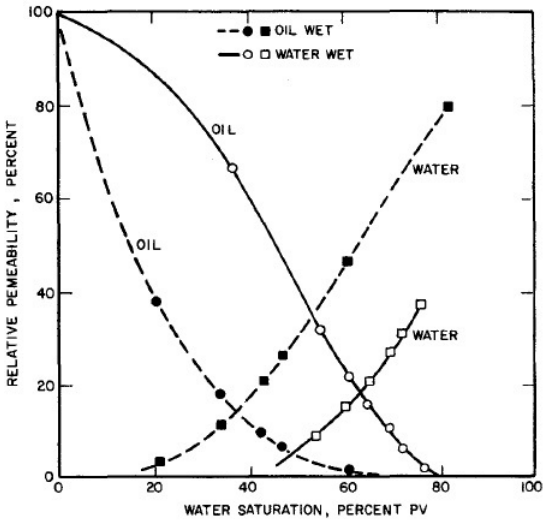


Figure 2.5: Steady-state oil/water relative permeabilities

## 2.6 Capillary pressure curves

Capillary pressure is defined as the pressure difference between the non-wetting phase and the wetting phase and is expressed by the following relation:

$$p_c = p_{nw} - p_n \tag{2.14}$$

In Eq. 2.14, $p_c$ is capillary pressure, $p_{nw}$ is pressure in the non-wetting phase, $p_n$ is pressure in the wetting phase. The magnitude of the capillary pressure depends on saturation of each phase, on the nature of the continuous phase, and on the distribution, shape, and size of the pores and pore throats. It is simpler to visualize the effect of capillary pressure in a capillary tube (Figure 2.6), capillary pressure in this geometry is given by:

$$p_c = \frac{2\sigma cos\theta}{r} \tag{2.15}$$

In Eq. 2.15, $\sigma$ is the interfacial tension between the two fluids, $\theta$ is the angle of contact which denotes the wettability of the capillary tube; and $r$ is the radius of the capillary tube. The angle of contact which denotes the wettability is shown in Fig. 2.6.

There are two types of capillary pressure processes: drainage and imbibition. In a drainage process, the non-wetting fluid displaces the wetting fluid, while the reverse occurs for imbibition [1]. It is possible to plot capillary pressure as a function of water saturation. Generally, there is hysteresis in capillary pressure as the saturation is varied, making drainage and imbibition curves different. An

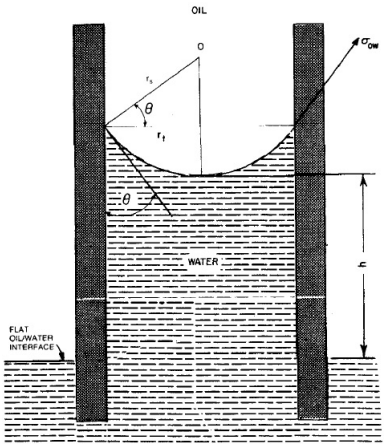


Figure 2.6: Oil/water interface in a capillary tube

example of capillary pressure curve as a function of water saturation for a water-wet system is presented in Fig.2.7 taken from [1].

Three sections can be distinguished in the capillary pressure curve of Fig. 2.7.

A drainage capillary pressure (curve 1) is measured by gradually increasing the capillary pressure from zero to a large positive value, which reduces the saturation of the wetting phase (water). As saturation is decreased, portions of the wetting phase become disconnected from the bulk wetting phase. Eventually, when the externally applied capillary pressure is sufficiently high, all of the wetting phase remaining in the core will be disconnected and the capillary pressure curve will be almost vertical [1]. Curve 2 of Fig. 2.7 is the spontaneous imbibition curve, determined after the drainage capillary pressure curve is measured. The capillary pressure, initially at a large positive value, is gradually decreased to zero allowing the wetting phase to imbibe. Curve 3 of Fig. 2.7 is the forced imbibition curve, where the capillary pressure is decreased from zero to a large negative value. When the capillary pressure is negative, the pressure in the wetting phase (water) is higher than the pressure in the non-wetting phase oil, forcing water into the core.

Capillary pressure measured in strongly oil-wet system is presented in Fig. 2.8 taken from [1]. The core where this measurements took place was first saturated with oil, then a drainage capillary pressure curve (curve 1) was measured by decreasing the capillary pressure to a large negative value. It is important to note that the curve is plotted vs. oil saturation and with negative capillary pressure plotted upward. The spontaneous imbibition curve (curve 2) is measured as the capillary pressure goes to zero [1].

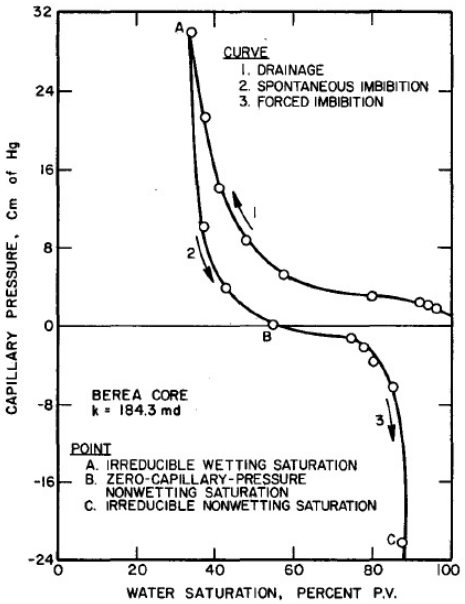


Figure 2.7: Oil/water capillary pressure curve measured on water-wet system

## 2.7 Leverett J function

It is often necessary to compare capillary pressure curves measured on different cores from the same reservoir. Because capillary pressure is affected by both permeability and porosity, it is necessary to correct for these effects before a proper comparison can be made. This is done with the empirical Leverett J function [16]:

$$J(S_w) = \frac{P_c}{\sigma}(\frac{k}{\phi})^{1/2} \tag{2.16}$$

Where $k$ is absolute permeability, $\phi$ is porosity, $P_c$ is capillary pressure, $\sigma$ is interfacial tension. All capillary pressure data from a formation will be reduced to a single curve when the Leverett J function is plotted vs. saturation [1].

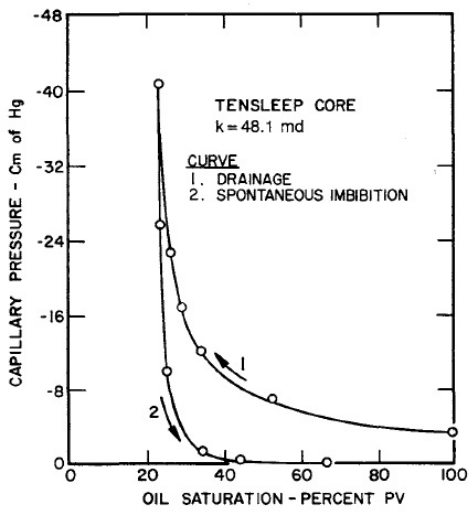


Figure 2.8: Oil/water capillary pressure curve measured on oil-wet system

## 2.8 Scaling in mathematics

The aim of scaling is to reduce the number of parameters in a given model. So, a pre-requisite of the technique of scaling is knowledge of the equations governing the system. To understand scaling as a tool for analysis of physical problems a simple example is discussed.

The movement of a body with mass $m$ in 1 dimension is illustrated in Fig. 2.9. The body is subjected to three forces: driving force $F_d$, spring force $F_s$ and friction with the surface $F_f$. According to Newton's second law following equation describes the position of the body respect with time.

$$m\frac{d^2u}{dt^2} = -F_f - F_s + F_d \tag{2.17}$$

Friction, spring and driving force are given by by:

$$F_f = c\frac{du}{dt} \qquad F_s = ku \qquad F_d = F_0 Sin(wt) \tag{2.18}$$

Where the driving force $F_d$ is taken harmonic with angular frequency $w$ and amplitude $F_0$. The force exerted by the spring $F_s$ is linearly proportional to the deviation $u$ (Fig. 2.9 b) measured respect to the equilibrium position (Fig. 2.9 a). The friction force $F_f$ is proportional to the velocity of the mass.

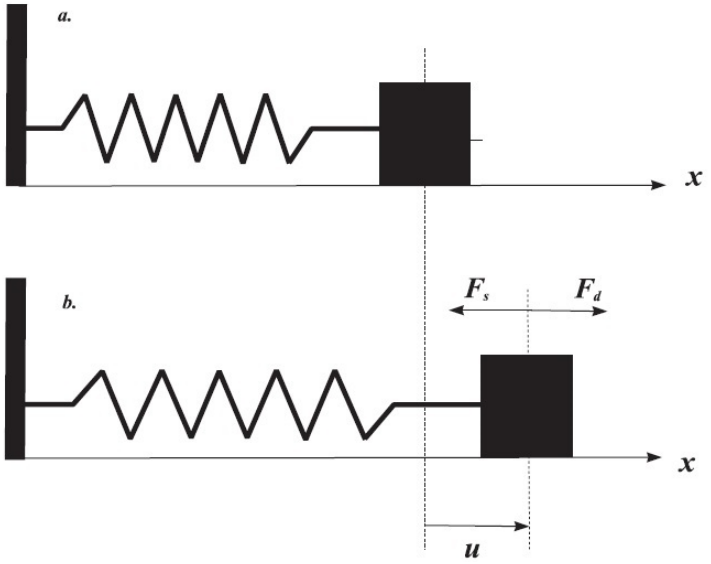


Figure 2.9: A vibrating mass attached to a spring

Replacing Eq. 2.18 in Eq. 2.17 and stating the initial conditions we have:

$$\begin{aligned} m\frac{d^2u}{dt^2} + c\frac{du}{dt} + ku &= F_0 Sin(wt) \\ u_0 = u(t_0) \qquad\qquad & v_o = \frac{du}{dt}(t_0) \end{aligned} \tag{2.19}$$

The problem (Eq. 2.19) has seven parameters $m$, $c$, $k$, $F_0$, $w$, $u_0$ and $v_0$, and two variables $u$ and $t$. Considering the scaling of variables:

$$\eta = \frac{x}{a} \qquad\qquad \tau = \frac{t}{b} \tag{2.20}$$

The problem from Equation 2.19 takes the form:

$$\frac{ma}{b^2}\frac{d^2\eta}{d^2\tau} + \frac{ca}{b}\frac{d\eta}{d\tau} + ka\eta = F_0 sin(w\tau) \tag{2.21}$$

Selecting $a = F_0/k$ and $b = \sqrt{m/k}$ we have the final equation:

$$\begin{aligned} \frac{d^2\eta}{d^2\tau} + c'\frac{d\eta}{d\tau} + \eta &= sin(w'\tau) \\ c' = c/\sqrt{km} \qquad & w' = w\sqrt{m/k} \end{aligned} \tag{2.22}$$

The initial parameters $u_0'$ and $v_o'$ should be scaled accordingly. The scaling procedure reduces the initial 7 parameters to only 4. Furthermore, to study the problem 2.22 we only need to vary the parameters $c'$ and $w'$. This same principle is applied in section 3.3 to reduce the number of variables describing the 1D+1D model.

# Chapter 3

# Model description

This chapter describes the construction of the 1D+1D model which is taken from [19].

## 3.1 Transport equations

The equations describing incompressible, immiscible oil-water flow in porous media are given by:

$$\partial_t(\phi S_o) = -\nabla(\phi V_o) \tag{3.1}$$

$$\partial_t(\phi S_w) = -\nabla(\phi V_w) \tag{3.2}$$

Where $\phi$ is porosity, $S$ is saturation, $V$ is pore velocity subscripts $o$ and $w$ represent oil and water phases. Darcy viscosity is given by $\phi V_i$.

$$\phi V_i = -K\lambda_i[\nabla p_i - \rho_i g \nabla z], \quad \lambda_i = \frac{k_{ri}}{\mu_i}, \quad (i = w, o) \tag{3.3}$$

Where $p_i$ is pressure, $\rho_i$ is density, $\lambda_i$ in mobility, $k_{ri}$ is relative permeability, $\mu_i$ is viscocity, $K$ is absolute permeability tensor, $z$ is positive direction upwards, and $g$ is the gravity acceleration. The saturations and pressures are constrained by the conditions:

$$S_w + S_o = 1, \quad p_c = p_o - p_w \tag{3.4}$$

where $p_c$ is capillary pressure. The capillary pressure function is considered known. Adding Eq.3.1 and Eq.3.2, using Eq.3.4 and the assumption that porosity is constant we have:

$$\partial_t(\phi(S_o + S_w)) = -\nabla.(\phi(V_o + V_w)) = -\nabla.(\phi(V_t)) = 0 \tag{3.5}$$

The fractional flow equation is defined as:

$$f_w = \frac{\lambda_w}{\lambda_w + \lambda_o} = \frac{\frac{k_{rw}}{\mu_w}}{\frac{k_{rw}}{\mu_w} + \frac{k_{ro}}{\mu_o}} \tag{3.6}$$

Using Eq. 3.3, Eq.3.4 and Eq.3.5, the total Darcy velocity is given by:

$$\phi(V_t) = -K(\lambda_o[\nabla p_o - \rho_o g \nabla z] + \lambda_w[\nabla(p_o - p_c) - \rho_w g \nabla z]) \tag{3.7}$$

Solving for $\nabla p_o$ and introducing $f_w$:

$$\nabla p_o = \frac{\lambda_o f_w \rho_o g \nabla z}{\lambda_w} + f_w \nabla p_c + f_w \rho_w g \nabla z - \frac{f_w \phi V_t}{\lambda_w K} \tag{3.8}$$

On the other hand combing Eq.3.2, Eq.3.3 and Eq.3.4:

$$\partial_t(\phi S_w) = -\nabla(-K\lambda_w[\nabla(p_o - p_c) - \rho_w g \nabla z]) \tag{3.9}$$

Replacing Eq.3.8 in Eq.3.9 and defining $\Delta\rho \equiv \rho_w - \rho_o$ the relation describing flow of oil and water in porous media is given by:

$$\partial_t(\phi S_w) + \nabla.(\phi V_t f_w(S_w) + Kg[\lambda_o f_w](S_w)\Delta\rho\nabla z) = -\nabla.(K[\lambda_o f_w](S_w)\nabla p_c(S_w)) \tag{3.10}$$

Eq.3.10 shows that the change in water saturation is affected by an advective gravitational term and a capillary diffusion term. The velocity field $V_t$ and $S_w$ (denoted $S$ in the following) are the variables to be calculated.

## 3.2 Fracture-matrix geometry

A combined fracture-matrix 1D+1D model is constructed in order to investigate the role of spontaneous imbibition (SI) as a recovery mechanism in an idealized geometry for different fracture-matrix flow regimes. The model considers flow along a single fracture from injector to producer well with porous matrix along the fracture being drained for oil as illustrated in Fig 3.1 taken from [19]. The fracture in considered as 1-dimensional entity and advection is neglected in the matrix.

The system is considered in the x-y plane consisting of a single fracture, surrounded by matrix on both sides in a symmetrical rectangular geometry, as illustrate in Fig. 3.1. The fracture is located along the y-axis, has length $L_y$ and width $2b$. The thickness of the matrix is $L_x$. The fracture and matrix domains are given by:

$$\begin{aligned} \Omega^f &= (x, y) : -2b < x < 0; 0 < y < L_y, \\ \Omega^M &= (x, y) : -2b - L_x < x < -2b, 0 < x < L_x; 0 < y < L_y \end{aligned} \tag{3.11}$$

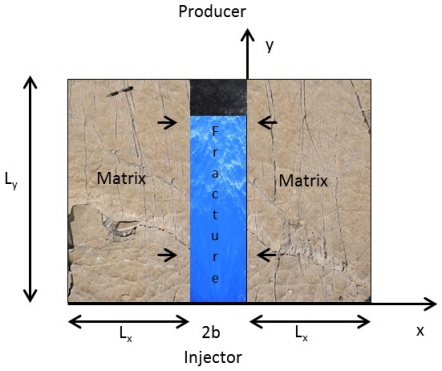


Figure 3.1: System geometry

The fracture and the matrix domains will have different properties in terms of permeability, porosity and flow functions. No-flow is considered at the outer boundaries of the matrix region. The fracture has an injector well at $y = 0$ and a producer well at $y = L_y$, these are given by:

$$\begin{aligned} \Gamma^{inj} &= (x, y) : -2b < x < 0; y = 0, \\ \Gamma^{prod} &= (x, y) : -2b < x < 0; y = L_y \end{aligned} \tag{3.12}$$

### 3.2.1 Matrix region

The matrix region is denoted with the superscript $M$. The model of Eq.3.10 is written for the matrix domain as ($\Omega^M$) as:

$$\partial_t(\phi^M S) = -\partial_x(K^M[\lambda_o^M f_w^M](S)\partial_x p_c^M(S)) - \partial_y(K^M[\lambda_o^M f_w^M](S)\partial_y p_c^M(S)) \tag{3.13}$$

Advective transport in the matrix is neglected (the terms associated with $V_t$ are neglected), gravity and flow in the z-direcion are also neglected.

### 3.2.2 Fracture region

The fracture region is denoted with the superscript $f$. The model of Eq.3.10 is written for the fracture domain

$$\partial_t(\phi^f S) = -\partial_x(K^f[\lambda_o^f f_w^f](S)\partial_x p_c^f(S)) - \partial_y(K^f[\lambda_o^f f_w^f](S)\partial_y p_c^f(S)) - \partial_y(\phi^f V_t^f f_w^f(S)) \tag{3.14}$$

Advective transport in the x-axis is neglected, gravity and flow in the z-direcion are also neglected. The fracture region is imagined as a plate with thickness 2b

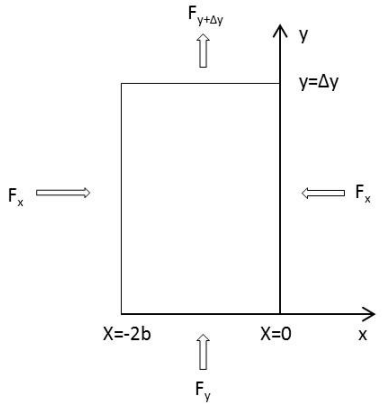


Figure 3.2: Differential element of the fracture

as shown in Fig.3.2. The mass transfer between the fracture and the matrix is considered as a source term $q_w$ that is positive when water enters the fracture. The model takes the form:

$$\partial_t(2b\phi^f S) = q_w - \partial_y(2bK^f[\lambda_o^f f_w^f](S)\partial_y p_c^f(S)) - \partial_y(2b\phi^f V_t^f f_w^f(S)) \tag{3.15}$$

Eq. 3.15, it is assumed that perfect mixing is achieved in the fracture width. The source term $q_w$ is is defined such that the flux entering the fracture corresponds to the diffusive flux leaving the matrix region from both sides. That is given by:

$$q_w = 2(-K[\lambda_o f_w](S)\partial_x p_c(S)) \mid_{x=0} \tag{3.16}$$

The transfer term Eq.3.16 is based purely on capillary motion due to a gradient in capillary pressure between the fracture and the matrix. The term is evaluated at the interface and must account for properties from both regions. Combining Eq. 3.15 and Eq. 3.16 we get the following 1D version of Eq. 3.14

$$\partial_t(\phi^f S) = -\frac{1}{b}(K[\lambda_o f_w](S)\partial_x p_c(S)) \mid_{x=0} -\partial_y(K^f[\lambda_o^f f_w^f](S)\partial_y p_c^f(S)) - \partial_y(\phi^f V_t^f f_w^f(S)) \tag{3.17}$$

## 3.3 Scaling the 1D+1D model

The model 1D+1D model is expressed in Eq.3.13 and 3.17.The model is scaled by using the following parameters:

$$x' = \frac{x}{L_x}, \quad x'_f = x'\frac{\phi^f}{\phi^M}, \quad y' = \frac{y}{L_y}, \quad t' = \frac{t}{\tau^f} \tag{3.18}$$

Introducing the parameters of Eq.3.18 in Eq.3.13 gives:

$$\frac{1}{\tau^f}\partial_{t'}(\phi^M S) = -\frac{1}{L_x^2}\partial_{x'}(K^M[\lambda_o^M f_w^M](S)\partial_{x'}p_c^M(S)) - \frac{1}{L_y^2}\partial_{y'}(K^M[\lambda_o^M f_w^M](S)\partial_{y'}p_c^M(S)) \tag{3.19}$$

Additionally the following dimensionless parameters and functions are introduced,

$$\mu' = \frac{\mu}{\mu_o}, \quad p_c'(s) = \frac{p_c(s)}{P_{x,max}} = J(s), \quad b' = \frac{b\phi^f}{L_x\phi^M}, \quad \lambda_i'(s) = \lambda_i(s)\mu_o \tag{3.20}$$

The following reference times are considered:

(i) Advetive flow in the fracture, $\tau^f = \frac{L_y}{v_T^f}(S)$

(ii) Capillary flow in the matrix, $\tau^{c,m} = \frac{\phi^M L_x^2 \mu_o}{k^m P_{c,max} D_{av}^M}(S)$

(iii) Capillary flow in the fracture, $\tau^{c,f} = \frac{\phi^f L_y^2 \mu_o}{k^f P_{c,max} D_{av}^f}(S)$

Note that $D_{av}$ is a dimensionless average of the scaled capillary diffusion coefficient $\lambda_o(S)f_w(s)J'(s)$ taken over the saturation range where water will flow [19].

$$D_{av} = \frac{1}{S_{eq} - S_0}\int_{S_0}^{S_{eq}} \lambda_o(S)f_w(s)\frac{dJ(s)}{ds}ds \tag{3.21}$$

Combining Eq.3.19 with parameters of Eq.3.20 the following equation is obtained:

$$\partial_{t'}(S) = -\frac{\tau^f K^M P_{c,max} D_{av}^M}{\phi^M L_x^2 \mu_o}\partial_{x'}(\frac{\lambda_o'^M f_w^M}{D_{av}^m}\partial_{x'}J^m) - \frac{\tau^f K^M P_{c,max} D_{av}^M}{\phi^M L_x^2 \mu_o}\frac{L_x^2}{L_y^2}\partial_{y'}(\frac{\lambda_o'^M f_w^M}{D_{av}^m}\partial_{y'}J^m) \tag{3.22}$$

From Eq.3.22 it is possible to note that a group of constants, introduction the following dimensionless number:

$$\alpha = \frac{\tau^f}{\tau^{c,m}} = \frac{L_y}{v_T^f}\frac{K^M P_{c,max} D_{av}^M}{\phi^M L_x^2 \mu_o} \tag{3.23}$$

Introducing the dimensionless parameter $\alpha$. Eq.3.22 is written:

$$\partial_{t'}(S) = -\alpha\partial_{x'}(\frac{\lambda_o'^M f_w^M}{D_{av}^M}\partial_{x'}J^M) - \alpha\frac{L_x^2}{L_y^2}\partial_{y'}(\frac{\lambda_o'^M f_w^M}{D_{av}^M}\partial_{y'}J^M) \quad (0 < x' < 0; 0 < y' < 1) \tag{3.24}$$

It is assumed that $\alpha\frac{L_x^2}{L_y^2} << 1$ such that capillary flow in y-direction is negligible. This is true if the water travels faster by advection in the fracture than by imbibition in the matrix in y-direction [19]. The 1D model for matrix flow takes the form of (the ' superscript is dropped):

$$\begin{aligned}\partial_t(S) &= -\alpha\partial_x(\frac{\lambda_o^M f_w^M}{D_{av}^M}\partial_x J^m)\\ &(0 < x < 0; 0 < y < 1)\end{aligned} \tag{3.25}$$

For the fracture 1D model, Eq.3.14 is combined with Eq.3.18, this gives:

$$\begin{aligned}\frac{1}{\tau^f}\partial_{t'}(\phi^f S) = -\frac{1}{L_x b}(K^M[\lambda_o^M f_w^M](S)\partial_{x'}p_c(S))\mid_{x=0} -\frac{1}{L_y^2}\partial_{y'}(K^f[\lambda_o^f f_w^f](S)\partial_{y'}p_c^f(S))\\ -\frac{1}{L_y}\partial_{y'}(\phi^f V_t^f f_w^f(S))\end{aligned} \tag{3.26}$$

Introducing Eq.3.20 in Eq.3.26 gives:

$$\partial_{t'}(S) = -\frac{L_x L_y K^M P_{c,max} D_{av}^M}{V_t^f \phi^M L_x^2 b\mu_o}(\frac{\lambda_o'^M f_w^M}{D_{av}^M}\partial_{x'}J^m)\mid_{x=0} -\frac{K^f P_{c,max} D_{av}^f}{V_t^f \phi^f L_y \mu_o}\partial_{y'}(\frac{\lambda_o'^f f_w^f}{D_{av}^f}\partial_{y'}J^f) - \partial_{y'}(f_w^f) \tag{3.27}$$

Introduction the dimensionless parameters

$$\beta = \frac{V^M}{V^f} = \frac{1}{b'} = \frac{L_x\phi^M}{b\phi^f} \qquad \gamma = \frac{\tau^f}{\tau^{c,f}} = \frac{K^f P_{c,max} D_{av}^f}{V_t^f \phi^f L_y \mu_o} \tag{3.28}$$

Introduction parameters $\beta$ and $\gamma$. Eq.3.27 is written:

$$\begin{aligned}\partial_{t'}(S) = -\alpha\beta(\frac{\lambda_o'^M f_w^M}{D_{av}^M}\partial_{x'}J^M)\mid_{x=0} -\gamma(\frac{\lambda_o'^f f_w^f}{D_{av}^f}\partial_{y'}J^f) - \partial_{y'}(f_w^f)\\ (-2/\beta < x < 0; 0 < y < 1)\end{aligned} \tag{3.29}$$

It is assumed that $\gamma << 1$ such that any capillary gradient in the fracture is negligible. The velocity in fracture is proportional to the fracture permeability, that is $V_t^f \propto K^f$. The capillary pressure as included in $D_{av}^f P_{c,max}$ varies with permeability according to Leverett J function (Eq.2.16). It follows that $\gamma \propto \frac{1}{L_y\sqrt{K^f}}$ and will become negligible for large $K^f$ [19]. The resulting equation takes the form (the ' superscript is dropped):

$$\begin{aligned}\partial_t(S) = -\alpha\beta(\frac{\lambda_o^M f_w^M}{D_{av}^M}\partial_x J^M)\mid_{x=0} -\partial_y f_w^f\\ (-2/\beta < x < 0; 0 < y < 1)\end{aligned} \tag{3.30}$$

The scaled model is summarized in Eq.3.25 and Eq.3.30.

## 3.4 Initial, boundary and interface conditions

In addiction to the transport equations, the initial conditions are set in the following form:

$$S(x, y, t = 0) = S_0(x, y) \tag{3.31}$$

Boundary conditions for the fracture at the injector is given by the composition of the injected fluid:

$$S(\Gamma^{inj}, t) = S_{inj} \tag{3.32}$$

The boundary at the producer is treated as a point on a semi-infinite axis, this is expressed as:

$$S(-2/\beta < x < 0, \infty, t) = S_\infty \tag{3.33}$$

The boundary at the exterior of the matrix is given by (no flow at both sides):

$$(\lambda_o^M f_w^M \partial_x J^M) \mid_{x=0} = 0 \tag{3.34}$$

At the interface between fracture and matrix, we assume continuity in capillary pressure, this is:

$$J^M \mid_{x=0} = J^f \mid_{x=0} \tag{3.35}$$

## 3.5 Relative permeability and capillary pressure functions

A normalized water saturation is given by

$$S^* = \frac{S - S_{wr}}{1 - S_{or} - S_{wr}} \tag{3.36}$$

Where $S_{wr}$ is residual water saturation, $S_{or}$ is residual oil saturation. The relative permeability curves to be used to with the 1D+1D model are Corey type correlations given by:

$$k_{rw}(S) = k_w^*(S^*)^{N_w}, \quad k_{ro}(S) = k_o^*(1 - S^*)^{N_o}, \quad S_{wr} < S < 1 - S_{or} \tag{3.37}$$

$N_w$ and $N_w$ are Corey exponent for water and oil respectively, $k_w^*$ and $k_o^*$ are end point permeabilities for water and oil respectively. In the fracture, the relative permeabilities are assumed to be linear:

$$k_{rw} = S, \quad k_{ro} = 1 - S \tag{3.38}$$

The oil-water capillary pressure curves are defined through a dimensionless function J of the form $p_c(S) = P_{c,max}J(S^*)$. The dimensionless function $J$ for the matrix is given by:

$$J^m(s) = \frac{a_1}{1 + K_1 S^*} - \frac{a_2}{1 + K_2(1 - S^*)} + b_1 \tag{3.39}$$

Curves are given by specifying parameters $a_i, b_1, k_i$ The capillary pressure at the fracture is assumed zero:

$$J^f(S) = 0 \tag{3.40}$$

## 3.6 1D+1D model plus linear transfer function

In this section, the coupling of a tranfer function $T$ with the 1D+1D model will be described.Using the model described in Eq. 3.10, and writing the equation for the matrix region described in equations 3.11. We have the following relation:

$$\partial_t(\phi^M S) = -\partial_x(K^M[\lambda_o^M f_w^M](S)\partial_x p_c^M(S)) - \partial_y(K^M[\lambda_o^M f_w^M](S)\partial_y p_c^M(S)) \quad (3.41)$$

For the fracture region we have:

$$\partial_t(\phi^f S) = -\partial_y(K^f[\lambda_o^f f_w^f](S)\partial_y p_c^f(S)) - \partial_y(\phi^f V_t^f f_w^f(S)) \quad (3.42)$$

If the fracture is considered as a 1 dimensional line of constant width $2b$, the equation can be written as:

$$\partial_t(2b\phi^f S) = -\partial_y(2bK^f[\lambda_o^f f_w^f](S)\partial_y p_c^f(S)) - \partial_y(2b\phi^f V_t^f f_w^f(S)) + 2T \quad (3.43)$$

Where T accounts for the transfer rate from the matrix to the fracture. T is positive when water enters the fracture.

### 3.6.1 Scaling the 1D+1D model plus linear transfer function

Scaling the previous equations in the same way as 1D+1D model in Section 3.3, we get for the matrix section:

$$\begin{gathered}\partial_t(S) = -\alpha\partial_x(\frac{\lambda_o^M f_w^M}{D_{av}^M}\partial_x J^m) \\ (0 < x < 0; 0 < y < 1)\end{gathered} \quad (3.44)$$

For the fracture section, the equation is slightly different from Eq. 3.30. The equation for the fracture section is derived in the following:

$$\frac{\phi^f}{\tau^f}\partial_{t'}(S) = -\frac{\phi^f V_T^f}{L_y}\partial_{y'}(f_w^f) - \frac{K^f}{L_y^2\mu_o}\partial_{y'}([\lambda_o^f f_w^f](S)\partial_{y'}(p_c^f)(S) + \frac{T}{b} \quad (3.45)$$

$$\partial_{t'}(S) = -\partial_{y'}(f_w^f) - \frac{\tau^f K^f P_{max} D_{av}}{\phi^f L_y^2\mu_o}\partial_{y'}(\frac{[\lambda_o^f f_w^f](S)}{D_{av}}\partial_{y'}(J^f)(S)) + \frac{\tau^f T}{\phi^f b} \quad (3.46)$$

When T takes the form of Eq. 2.10 and we drop the ' symbol, we have:

$$\partial_t(S) = -\alpha(\frac{\phi^M L_x^2 \mu_o}{\phi^f b K^M P_{max}}) B\phi^M (S_{eq}^M - S_w^M) - \partial_y f_w^f \qquad (-2/\beta < x < 0; 0 < y < 1) \tag{3.47}$$

## 3.7 MATLAB program for the 1D+1D numerical model

A programming language is required to implement the discretized equations and solve them numerically. In this case MATLAB (matrix laboratory) program was chosen [19]. MATLAB is a multi-paradigm numerical computing environment and fourth-generation programming language. Developed by MathWorks, MATLAB allows matrix manipulations, plotting of functions and data, implementation of algorithms, creation of user interfaces, and interfacing with programs written in other languages, including C, C++, Java, and Fortran.

MATLAB was chosen because its easiness to handle matrices and numerical loops compared to programs like Excel. Moreover, the flexibility it offers to change the wettability of the rock and to plot the results.

# Chapter 4

# Numerical investigations of the 1D+1D model

As discussed in Chapter 1, the problem addressed is to understand the factors affecting spontaneous imbibition by the use of a 1D+1D model and to test the linear transfer function presented in Section 2.2.1. In this section, the 1D+1D model will be used to understand the parameters affecting fracture matrix flow. The 1D+1D model has been discretized and solved using a operator splitting approach as explained in detail in [19]. The solution of the 1D+1D model has been implemented into a MATLAB code. A schematic of the solution procedure is presented in Fig. 4.1.

The MATLAB code is run changing the input parameters to identify their effect on the output plots. As described in Chapter 3, the displacement of oil by water takes place in a two dimensional geometry. Transport due to advection takes place in the fracture and capillary forces influence flow in the direction perpendicular to the fracture. First, The input parameters are presented.

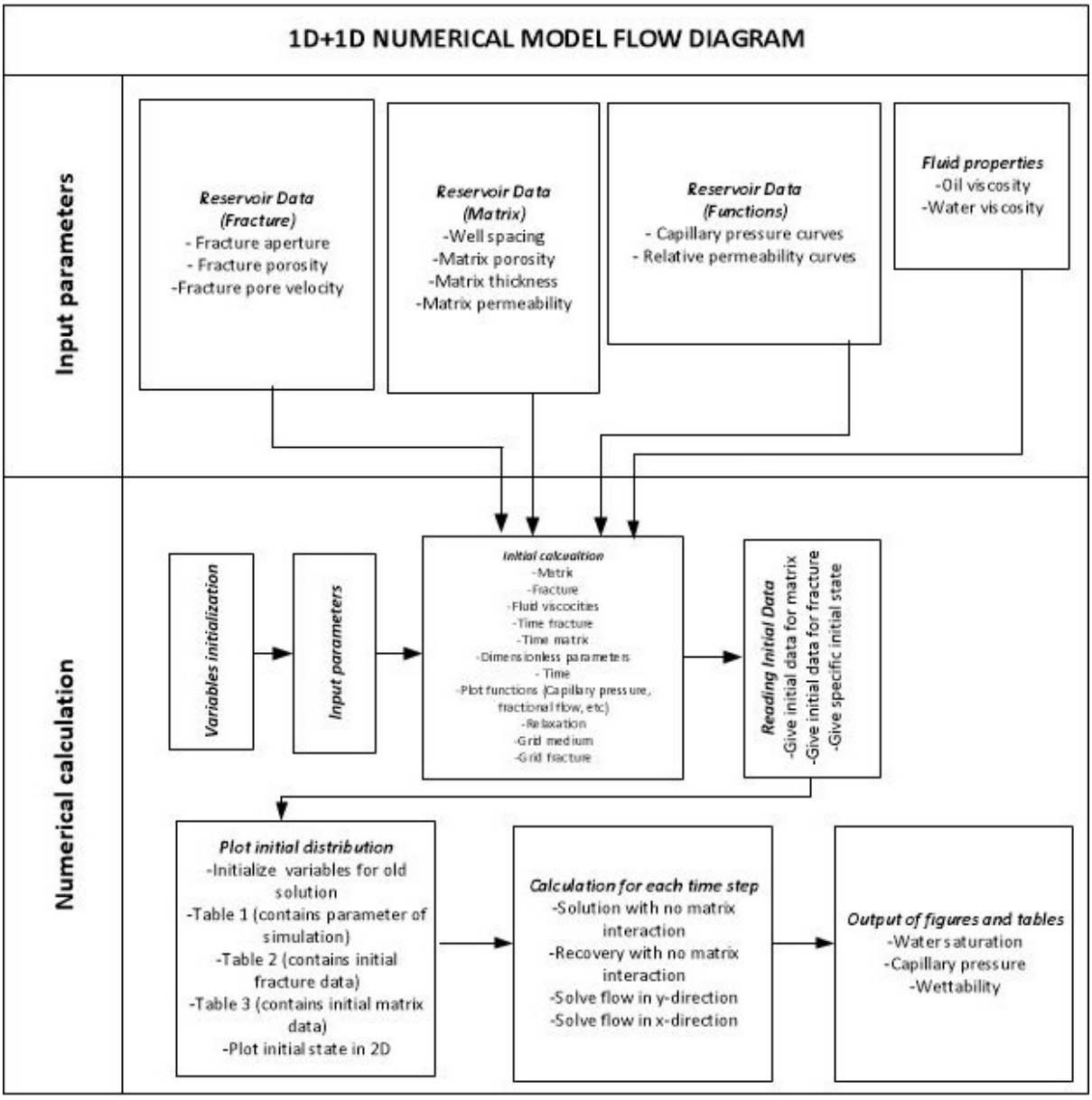


Figure 4.1: 1D+1D Numerical model solution procedure

## 4.1 Input parameters

The parameters required to use the numerical calculations of the 1D+1D model are: Well spacing $L_y$, Fracture aperture $2b$, Fracture porosity $\phi^f$, Matrix porosity $\phi^m$, Matrix thickness $L_x$, Fracture pore velocity $v_T^f$, Matrix permeability $K^m$, Oil viscosity $\mu_o$, Water viscosity $\mu_w$ and Initial capillary pressure $P_{c,max}$. These values are summarized in Table 4.1.

Table 4.1: Reservoir and fluid information

| | |
|---|---|
| Well spacing $L_y$ | 100 m |
| Fracture aperture $2b$ | 0.001 m |
| Fracture porosity $\phi^f$ | 1 |
| Matrix porosity $\phi^m$ | 0.2 |
| Matrix thickness $L_x$ | 0.05 m |
| Fracture pore velocity $v_T^f$ | 10 m/d |
| Matrix permeability $K^m$ | 5 mD |
| Oil viscosity $\mu_o$ | 1 cp |
| Water viscosity $\mu_w$ | 1 cp |
| Initial capillary pressure $P_{c,max}$ | 120 pa |

It is also required to provide the capillary pressure curves for the matrix and fracture. These are presented in Fig. 4.2. In this figure, the blue curve represents the capillary pressure function when the rock is preferentially water wet (PWW) and the red curve for preferentially oil wet (POW). The green line is the capillary pressure in the fracture. The behaviour shows agreement with the concepts presented in Section 2.6. This curves are qualitative in nature and do not give an exact representation of wettability since they are not based on experimental measurements or derived from pore scale simulations [19]. Eq. 3.39 was used to generate these capillary pressure curves for the matrix and Eq. 3.40 was used for the fracture. The parameters used in this equations are presented in Table 4.2.

Table 4.2: Input parameters for matrix scaled capillary pressure function $J^m$

| | $A$ | $B$ | $k_1$ | $k_2$ | $b_1$ |
|---|---|---|---|---|---|
| Pref. Oil-Wet | 1 | -1 | 30 | 40 | -0.22 |
| Pref. Water-Wet | 1 | -1 | 30 | 40 | 0.20 |

Relative permeability functions for the matrix and fracture are also required, they are presented in Fig. 4.3. In this figure, the blue curves represents the relative permeability when the system is preferentially water wet (PWW) and the red curve when the system is preferentially oil wet (POW). The green lines are

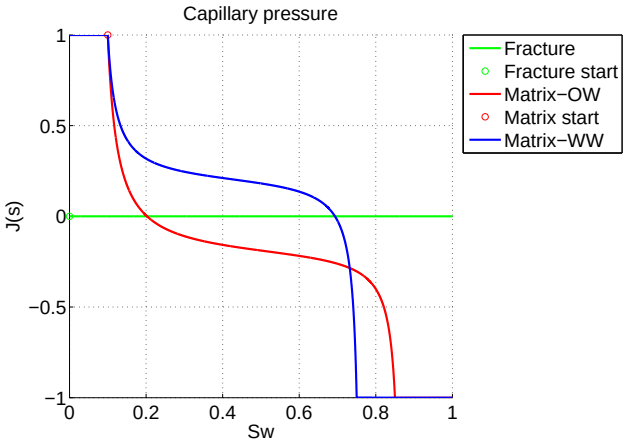


Figure 4.2: Capillary pressure functions

the relative permeabilities in the fracture. The behaviour of these curves shows agreement with the concepts presented in Section 2.5. This curves are qualitative in nature and do not give an exact representation of relative permeabilities since they are not based on experimental measurements. Eq. 3.37 was used to generate these relative permeability curves for the matrix and Eq. 3.38 was used for the fracture, the parameters used in this relation are presented in Table 4.3.

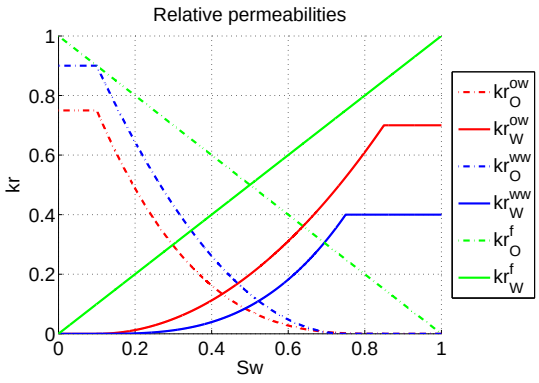


Figure 4.3: Relative permeabilities functions

The initial water saturation in the matrix is $s_0^M = 0.10$, at which the capillary pressure takes the highest value $J^M(s_0^M) = 1$. The initial water saturation in the fracture is $s_0^f = 0.0$ (because any initial water would imbibe in the matrix) at which the capillary pressure in the fracture is zero, $J^f(s_0^f) = 0$.

The following numerical calculations were made by dividing the matrix block

Table 4.3: Input parameters for Corey type relative permeability functions

| | $k_w^*$ | $N_w$ | $k_o^*$ | $N_o$ | $S_{wr}$ | $S_{or}$ |
|---|---|---|---|---|---|---|
| Pref. Oil-Wet | 0.7 | 2.0 | 0.75 | 3.0 | 0.10 | 0.15 |
| Pref. Water-Wet | 0.4 | 3.0 | 0.9 | 2.0 | 0.10 | 0.25 |

along the x-axis in 10 parts, that is $N_x = 10$ cells. In similar way the fracture along the y-axis was divided in 30 parts, that is $N_y = 30$.

## 4.2 Preferentially water-wet

In this section the case when the rock is preferentially water-wet is described, the PWW system is considered the base case, additionally the parameters of Table 4.1 are used. For this base case the scaled capillary diffusion coefficient (SCDC) is plotted as function of saturation, and the average SCDC is taken between the initial saturation $S_0 = 0.1$ and the equilibrium saturation $S_{eq} = 0.7$. This is shown in Figure 4.4(The absolute value is taken). The following parameters are calculated for the this case using the 1D+1D model:

$$D_{av,0} = 0.0120,\ \Delta S^{MPWW} = 0.6,\ \tau_0^f = 10d,\ \tau_0^M = 804d,\ \alpha_0 = 0.0124\ \beta_0 = 20,\ \frac{\mu_w}{\mu_o} = 1 \tag{4.1}$$

$\tau_0^f$ and $\tau_0^M$ are calculated with relations stated in Section 3.3. Parameters $\alpha_0$ and $\beta_0$ are calculated with Eq. 3.23 and Eq. 3.28 respectively. $\Delta S$ is the imbibition potential which is calculated as $\Delta S = S_{eq} - S_0$.

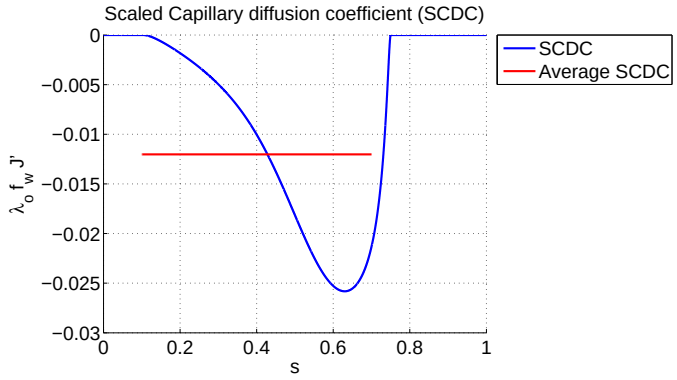


Figure 4.4: Scaled capillary diffusion coefficient PWW

## 4.3 Preferentially oil-wet

In this section the case when the rock is preferentially oil-wet is described, additionally the parameters of Table 4.1 are used. For this case the scaled capillary diffusion coefficient (SCDC) is plotted as function of saturation, and the average SCDC is taken between the initial saturation $S_0 = 0.1$ and the equilibrium saturation $S_{eq} = 0.2$. This is shown in Fig. 4.5(The absolute value is taken). The following parameters are calculated for the this case:

$$D_{av,0} = 0.0152,\ \Delta S^{mPOW} = 0.1,\ \tau_0^f = 10d,\ \tau_0^m = 634,5d,\ \alpha_0 = 0.0157\ \beta_0 = 20,\ \frac{\mu_w}{\mu_o} = 1 \tag{4.2}$$

These values have been calculated in the same way as for the PWW case.

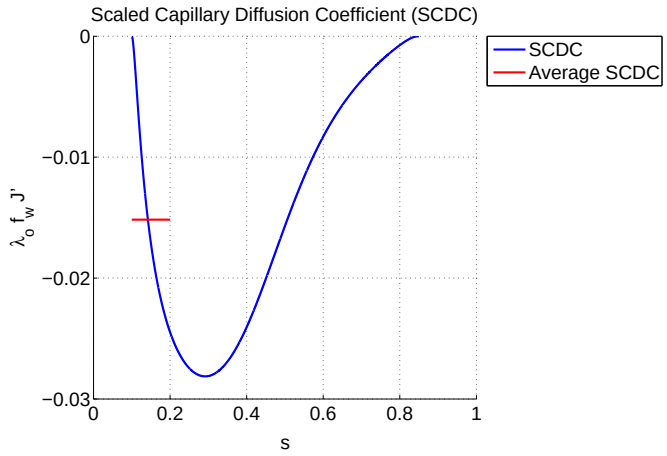


Figure 4.5: Scaled capillary diffusion coefficient POW

## 4.4 Influence of rock wettability

In this section, the influence of rock wettability on water saturation, total oil recovery and capillary pressure is evaluated. As previously stated, the base case is when the rock is PWW and will be compared to the case when the rock is POW. A fracture volume (FV) is defined as FV= $2bL_y$. When injecting 1 FV and no fracture matrix interaction occurs, the water front should reach the producer well. However, the model shows that imbibition delays the water front. The water front is delayed to a different rate when the rock is PWW opposed to POW. This is

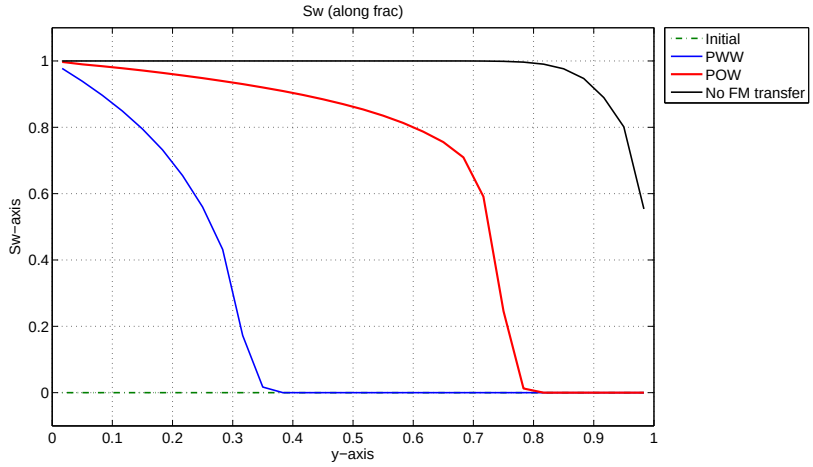


Figure 4.6: Water saturation along the fracture after injecting 1 FV

depicted in Fig. 4.6. Since more water is retained in the PWW matrix, higher delay of the water front is observed in this case.

The effect of rock wettability on oil recovery is depicted in Fig. 4.7 after injecting 1 RPV (RPV $= \phi^f 2bL_y + 2\phi^M L_x L_y$). More oil is recovered in PWW opposed to the POW case. This is related to the imbibition potential $\Delta S$ which is greater in the PWW case. In the PWW case water imbibes in the matrix during a longer time compared to the POW. When water imbibes in the matrix it displaces oil to the fracture, subsequently the water displaces the oil in the fracture towards the producing well. Hence the greater recovery in the PWW case.

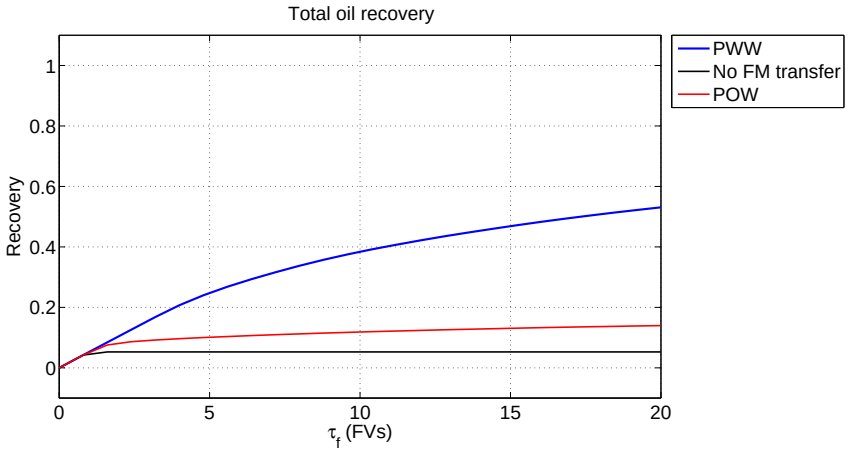


Figure 4.7: Oil recovery after injecting 1 RPV

The water saturation along the matrix at the injector well for PWW and POW is presented in Fig. 4.8, clearly the water saturation in the matrix is higher in the PWW than in the POW case. In PWW case more water is imbibed because of higher capillary pressure.

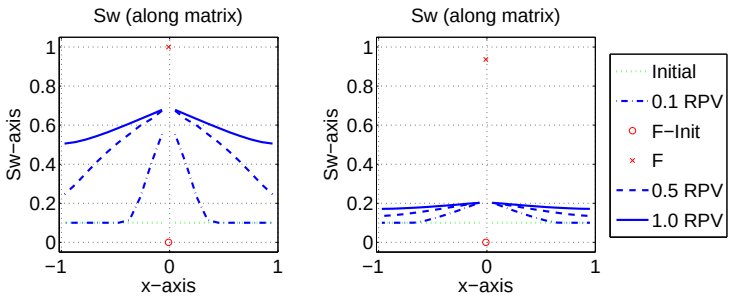


Figure 4.8: Water saturation along matrix PWW(left) and POW (rigth)

Fig. 4.9 shows the capillary pressure along the matrix at the injector well for the PWW and POW cases. The capillary pressure for different injected volumes in shown. As water imbibes in the PWW case capillary pressure reduces, reducing the flow of water inside the matrix. As injected volume increases, the capillary pressure along the matrix is reduced.

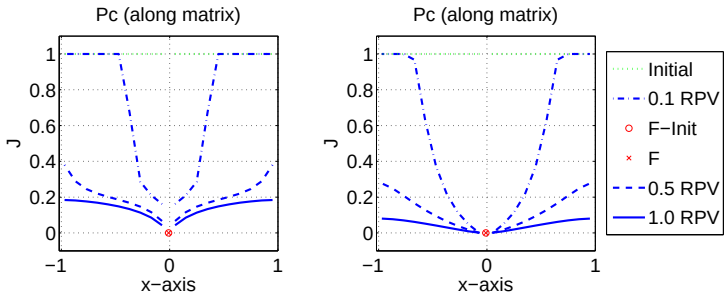


Figure 4.9: Capillary pressure along matrix PWW(left) and POW (rigth)

The water saturation at different injected volumes is presented in Fig. 4.10, this figure illustrates the effect of advection and imbibition. Initially the water spreads into the reservoir in a bell shape. As the water front travels trough the reservoir, the imbibition rate goes down, hence some oil stays stored in the matrix. This figure shows the same qualitative behaviour achieved in experimental work described in [20] where a Computer Tomography scanner was used to study the

flow of water and air in a fracture-matrix geometry similar to the considered by the 1D+1D model.

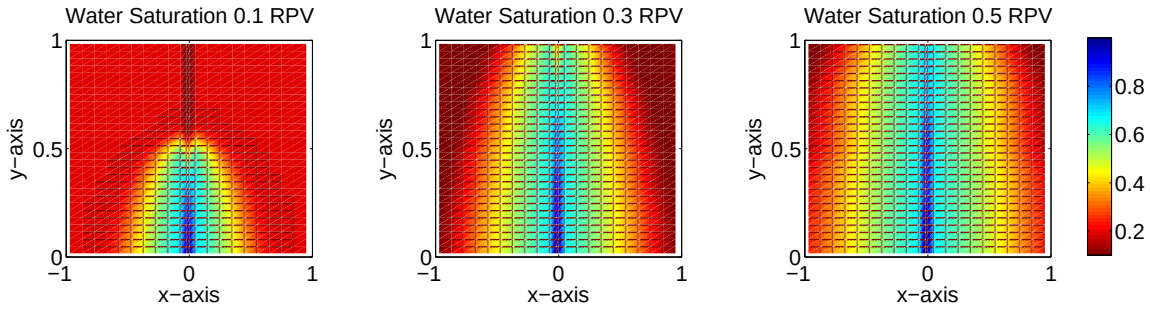


Figure 4.10: Water saturation PWW at different injected volumes left:0.1 RPV, midle:0.3 RPV, rigth: 0.5 RPV

Capillary pressure is the driving force imbibing water into the matrix and displacing oil to the fracture. Capillary pressure at different injected volumes can be seen in Fig. 4.11. As more water is injected, the difference in capillary pressure between the fracture and the matrix reduces. This reduction in capillary pressure difference reduces the imbibition rate.

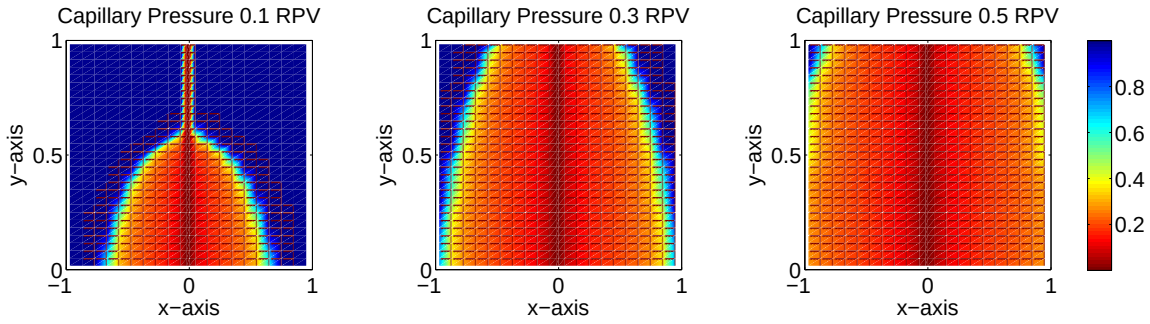


Figure 4.11: Capillary pressure PWW rock at different injected volumes left: 0.1 RPV, midle: 0.3 RPV, rigth : 0.5 RPV

## 4.5 Influence of parameter $\alpha$

The importance of Parameter $\alpha$ is discussed in this section. This parameter was introduced in section 3.3 after scaling the 1D+1D model, and it is described by Eq. 3.23. Parameter $\alpha$ is directly proportional to the magnitude of capillary forces and is crucial for the imbibition process. The importance of this parameter is evident from Fig. 4.12 and Fig. 4.13. To generate these figures the time describing the capillary flow in the matrix $\tau^{c,m}$ was modified by adjusting the initial capillary pressure $P_{c,max}$ to produce different values of $\alpha$ but keeping $\beta$ fixed.

Fig. 4.12 left shows the strong influence of parameter $\alpha$ on the water front in the fracture. After injecting 0.1 RPV, the simulation with $10.0\alpha_0$ shows water front delay in the fracture compared to the one with $0.1\alpha_0$. This is because higher capillary pressure difference and more imbibition takes place in the case of $10.0\alpha_0$.

When $\alpha$ is large, the oil recovery curves (middle Fig. 4.12) show a linear part followed by non-linear behaviour. When $\alpha$ is small, only non-linear behaviour is seen. These two different behaviours correspond to two regimes, the "filling fracture" and the "instantly filled" regimes [20]. When $\alpha$ is small, we have an "instantly filled" regime, the fracture is rapidly filled with water and little imbibition takes place. On the other hand, when $\alpha$ is large we have the "filling fracture" regime, in this case the fracture is slowly filled with water and large amount of water imbibes in the matrix.

For small $\alpha$, the relation between oil recovery and the square root of time is linear (right Fig. 4.12). This observation is consistent with experimental observations in [20] where the same behaviour is seen for the "instantly filled" regime in an oil-water system.

In the model we see that lower injection rate increases $\alpha$. According to Eq. 3.23, a reduction in the water injection rate by reducing $V_t^f$ will generate higher total oil recovery (middle Fig. 4.12). A lower injection rate represents a more efficient uptake of water by the matrix.

When $\alpha$ is small, the water will flow through the fracture and only the nearest matrix region is affected (left Fig. 4.13) This generates early water breakthrough and low total oil recovery.

When $\alpha$ is big, the water will imbibe deep in the matrix and all the matrix region is affected (right Fig. 4.13) This generates delayed water breakthrough and high total oil recovery.

## 4.6 Influence of parameter $\beta$

In this section, the influence of parameter $\beta$ on water saturation along the fracture and total oil recovery is studied.

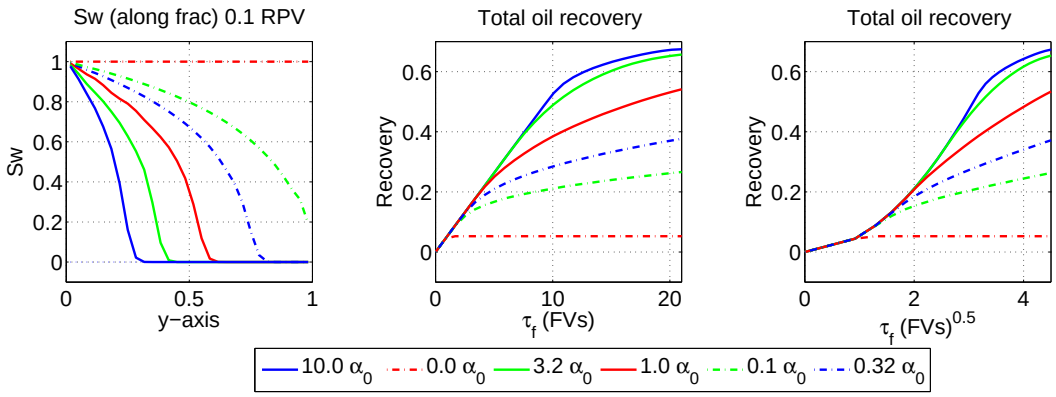


Figure 4.12: Influence of parameter $\alpha$, left:after injecting 0.1 RPV, middle: oil recovery as a function of time after injecting 1 RPV, right: oil recovery as a function of square root of time after injecting 1 RPV

Table 4.4: Time for injecting 1 RPV when changing $\beta$

| Fracture Aperture $2b$ $m$ | $\beta$ | $\alpha$ | $v_t^f$ $m/d$ | RPV $m^2$ | Injection Rate $m^2/d$ | Time to inject 1 RPV $d$ |
|---|---|---|---|---|---|---|
| 0.00025 | 80 | 0.0125 | 10 | 2.025 | 0.0025 | 810 |
| 0.001 | 20 | 0.0125 | 10 | 2.1 | 0.01 | 210 |
| 0.002 | 10 | 0.0125 | 10 | 2.2 | 0.02 | 110 |

According to Eq. 3.28, parameter $\beta$ can be changed by adjusting the fracture width $2b$. For the base case (Table 4.1) we have $2b_0 = 0.001\ m$ and $v_t^f = 10\ m/d$. The reservoir pore volume for the base case is:

$$RPV = \phi^f 2bL_y + 2\phi^m L_x L_y = 1 * 0.001 * 100 + 2 * 0.2 * 0.05 * 100 = 2.1m^2 \tag{4.3}$$

The time required to inject 1 RPV is given by:

$$t = \frac{RPV}{v_t^f * 2b} = \frac{2.1}{10 * 0.001} = 210d \tag{4.4}$$

If the fracture width $2b$ is changed, the time required to inject 1 RPV will also change, as shown in Table 4.4, the calculations were made in the same way as for the base case. It is important to note that parameter $\beta$ changes while $\alpha$ remains constant.

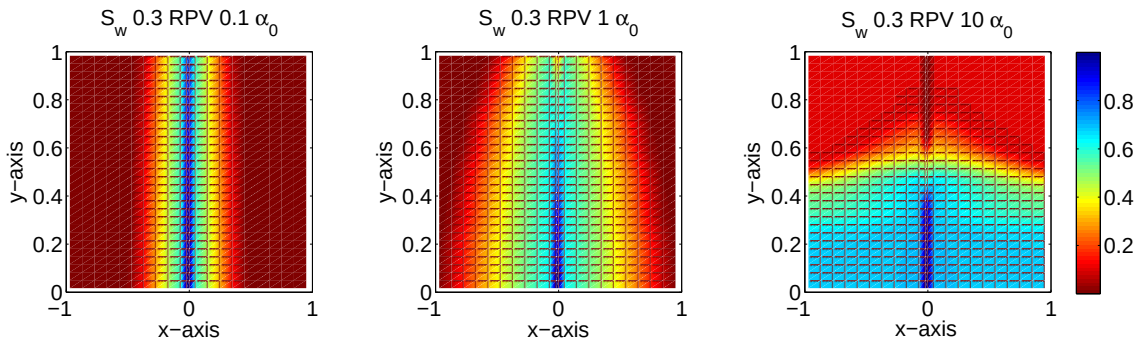


Figure 4.13: Influence of parameter $\alpha$ on water saturation after injecting 0.3 RPV, left: $0.1\alpha_0$ , middle: $1.0\alpha_0$, right: $10.0\alpha_0$

Total oil recovery when changing parameter $\beta$ is shown in Fig. 4.14, it is noted that the bigger $\beta$ is, higher oil recovery is achieved. The main reason for this behaviour is because there is more time for imbibition to occur. However, this considers that the injection rate is not constant (see Table 4.4).

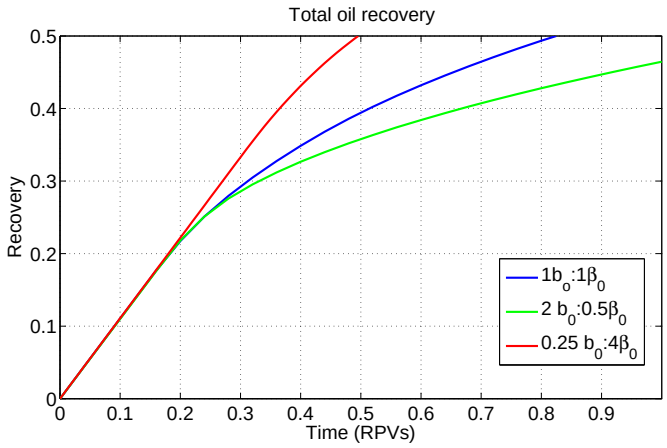


Figure 4.14: Influence of parameter $\beta$ on total oil recovery when $\alpha$ is kept constant

On the other hand, Fig. 4.15 shows the oil recovery when varying $\beta$, but at a constant injection rate. The details are shown in Table 4.5. It is noted that the larger *beta* is, lower oil recovery is achieved. In other words, at constant injection rate, when the fracture width $2b$ is small the oil recovery is smaller than when

fracture width is large.

The results are consistent with experimental observations in [20]. In this experimental studies with water and air, it was found that low water was imbibed when the fracture width is small, defining this condition as the "Instantly filled fracture" regime. When the fracture width is large, higher imbibition rates are achieved. This condition was defined as "Filling fracture" regime.

Table 4.5: Oil recovery changing fracture width and constant injection rate

| Fracture Aperture $2b$ $m$ | $\beta$ | $\alpha$ | $v_t^f$ $m/d$ | RPV $m^2$ | Injection Rate $m^2/d$ | Time to inject 1 RPV $d$ |
|---|---|---|---|---|---|---|
| 0.00025 | 80 | 0.0031 | 40 | 2.025 | 0.01 | 202.5 |
| 0.001 | 20 | 0.0125 | 10 | 2.1 | 0.01 | 210 |
| 0.002 | 10 | 0.0250 | 5 | 2.2 | 0.01 | 220 |

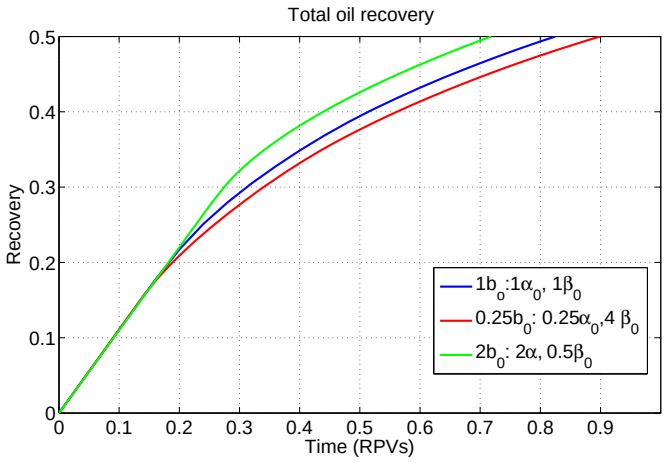


Figure 4.15: Influence of parameter $\beta$ on total oil recovery when the injection is constant 0.01 $m^2/d$

## 4.7 Influence of viscosity ratio

In this section the influence of viscosity ratio ($M = \mu_w/\mu_o$) is evaluated. Oil viscosity is involved in parameter $\alpha$ as given by Eq. 3.23, so water viscosity is changed to keep $\alpha$ and $\beta$ unchanged. The reference case ($\mu_w/\mu_o = 1$) is compared

to the cases of high viscosity ratio ($\mu_w/\mu_o = 1$) and low viscosity ratio ($\mu_w/\mu_o = 1/5$).

The change in viscosity ratio will affect the fractional flow function given by Eq. 3.6, the effect is shown in Fig. 4.16. Decreasing water viscosity increases the value of $f_w^M$ and $f_w^f$. The derivative of fractional flow function is affected by the viscosity change according to Fig. 4.17.

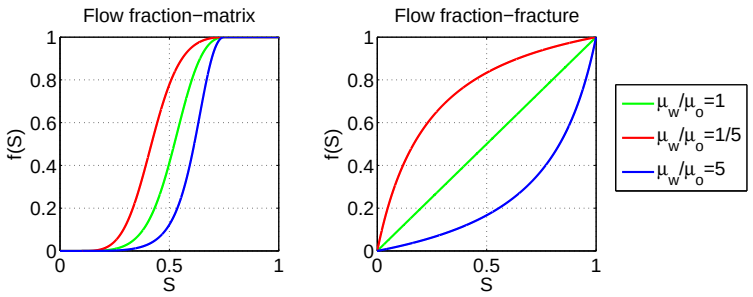


Figure 4.16: Effect of viscosity ratio change on Fractional Flow function, left: for the matrix, right: for the fracture

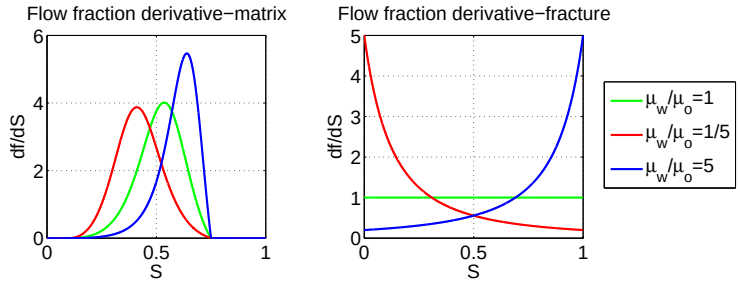


Figure 4.17: Effect of viscosity ratio on Fractional Flow function derivative, left: for the matrix, right: for the fracture

When the mobility ratio is low ($\mu_w/\mu_o = 1/5$) two important observations can be made.

The first one is that displacement of oil in the fracture is not as affective as in the base case ($\mu_w/\mu_o = 1$). This can be seen in Fig. 4.19, the water front, inside the fracture after injecting 1 FV, smears out compared to the base case.

The second one is that the capillary diffusion coefficient increases as shown in Fig. 4.18. Increasing the capillary diffusion coefficient improves the imbibition process.

In an un-fractured reservoir a high mobility ratio has a positive effect on recovery in the sense that water pushes the oil toward the producer in a piston like manner resulting in late water breakthrough [19]. In a fractured reservoir, reducing the viscosity ratio seems to improve the imbibition process. This is because the water phase is more mobile and imbibes into the matrix easily.

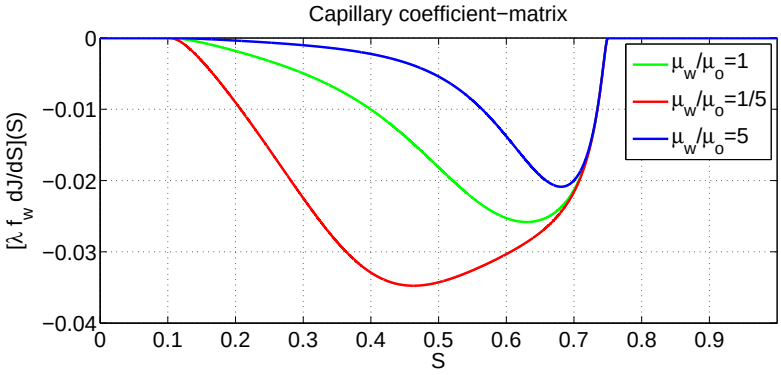


Figure 4.18: Influence of viscosity ratio on capillary diffusion coefficient

When the mobility ratio is high ($\mu_w/\mu_o = 5$) two important observations can be made.

The first one is that the displacement of oil in the fracture is more effective than the base case ($\mu_w/\mu_o = 1$). This can be seen in Fig. 4.19, the water front, inside the fracture after injecting 1 FV, sharpens compared to the base case.

The second one is that the capillary diffusion coefficient decreases as shown in Fig. 4.18. Decreasing the capillary diffusion coefficient worsens the imbibition process. Reducing the amount of oil displaced to the fracture by imbibition.

The water front in fracture is shown in Fig. 4.19 and Fig. 4.20 considering the process with and without imbibition respectively. The reduction in viscosity ratio smears out the water front in the fracture showing that water imbibes in the matrix. Increasing the viscosity ratio sharpens the water front improving oil displacement in the fracture.

Fig, 4.21 left shows the water saturation in the fracture matrix geometry after injecting 0.3 RPV when the viscosity ratio is low. Water spreads deep into the matrix and the water front in the fracture is limited to less than half the fracture length.

Fig. 4.21 right shows the water saturation in the fracture matrix geometry after injecting 0.3 RPV when the viscosity ratio is high. Water spreads half the matrix width into the matrix and the water front in the fracture reaches the producing well.

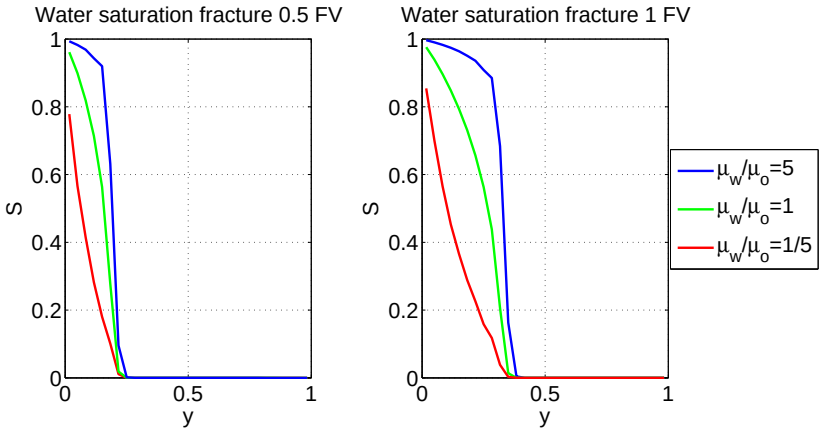


Figure 4.19: Influence of viscosity ratio on water front in the fracture with imbibition, left: after injecting 0.5 RPV, right: after injecting 1.0 RPV

A conclusive picture of the oil recovery as a function of viscosity ratio is presented in Fig. 4.22. It seems to be beneficial to reduce the water viscosity to increase oil recovery. This is contrary to the case of un-fractured reservoir where increase in water viscosity improves oil recovery. The main reason for this behaviour is that more water is imbibed when water viscosity is low, hence displacing more oil to the fracture and the production well.

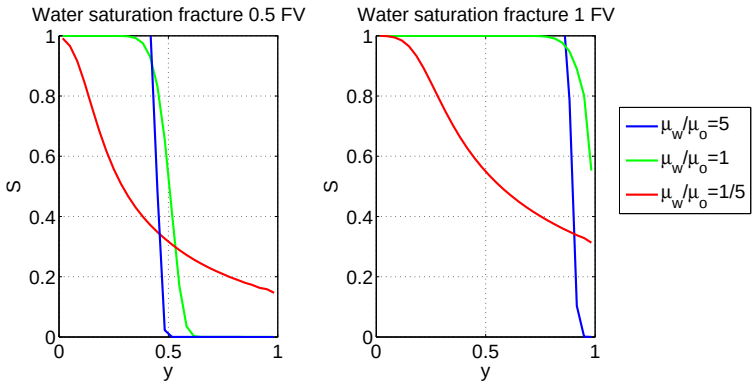


Figure 4.20: Influence of viscosity ratio on water front in the fracture without imbibition, left: after injecting 0.5 RPV, right: after injecting 1.0 RPV

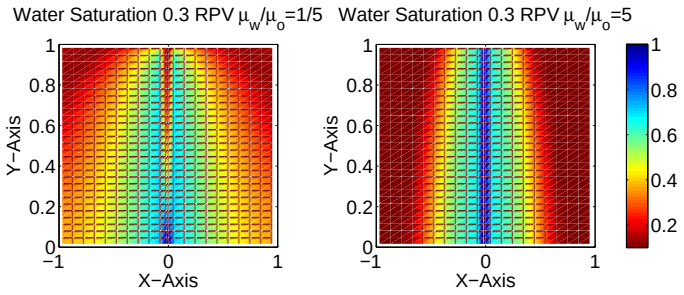


Figure 4.21: Effect of viscosity ratio on water saturation after injecting 0.3 RPV, left: $\mu_w/\mu_o = 1/5$, right: $\mu_w/\mu_o = 1/5$

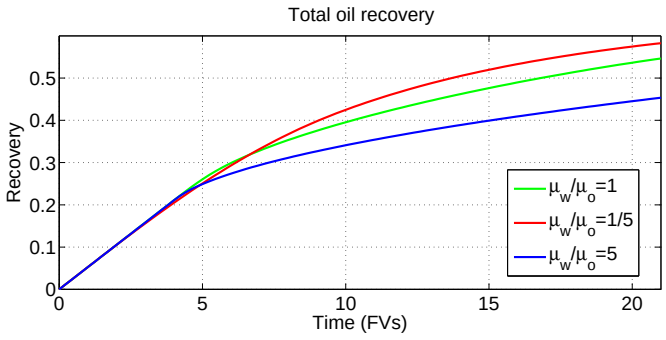


Figure 4.22: Influence of viscosity ratio on oil recovery

# Chapter 5

# Linear transfer function testing

## 5.1 Comparing the 1D+1D model to the linear transfer function model in PWW system

In this section the 1D+1D model described by Eq. 3.25 and Eq. 3.30 will be compared to the linear transfer function model described by Eq. 3.44 and Eq. 3.47 (LTF is used in the figures to denote the linear transfer function model). To make this comparison, all constants for the base case are used as given in Table 4.1. The saturation curves for the PWW case are used. 10 grid cells are used along x-direction in the matrix and 30 grid cells are used along the fracture.

Fig. 5.1 shows the oil recovery calculated with the linear transfer function and the 1D+1D model, after injecting 1 RPV. Various values of $B$ constants have been used ($B = 4E-8$, $6E-8$ and $9E-8$). The recovery calculated with the linear transfer function when $B = 6E-8$ matches closely the recovery calculated with the 1D+1D model. However, at early time, the linear transfer function over predicts the recovery. Furthermore, the linear transfer function predicts slightly lower recovery after injecting 2.5 FV's. It is possible to see that for $B = 9E-8$ the oil recovery is lower than for $B = 4E-8$, which means that the oil recovery is inversely proportional to the rate constant $B$.

Fig. 5.2 shows oil recovery at early time. In this picture, it is possible to appreciate a mismatch between the two models. The 1D+1D model shows linear behaviour before breakthrough, but the linear transfer function fails to reproduce this behaviour. This is because the linear transfer function considers the recovery as an exponential function of time (Section 2.2.1).

Fig. 5.3 shows a comparison when 1 FV has been injected. For various values of $B$ constant. The figure shows a close match between the linear transfer function and the 1D+1D model when $B = 6E-8$. The close match means that the rate at which water imbibes in the matrix is similar in both models. When $B > 6E-8$, the

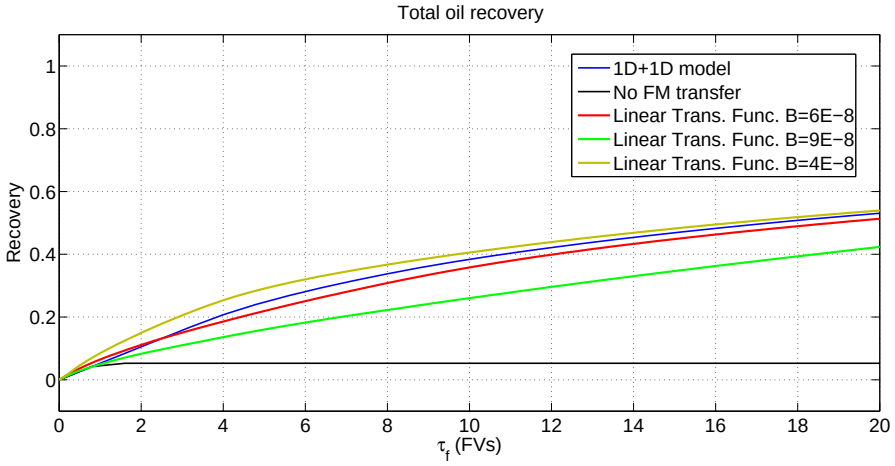


Figure 5.1: Oil recovery after injecting 1 RPV when using linear transfer function in PWW system

imbibition is higher than the predicted by the 1D+1D model, and when $B < 6E{-}8$ the imbibition is lower than the predicted by the 1D+1D model.

Fig. 5.4 shows the water saturation in the fracture matrix geometry calculated with the linear transfer function (LTF) at the top and the 1D+1D model at the bottom. Both models calculate similar water saturations in the fracture matrix geometry.

Additionally, the water saturation and capillary pressure in the matrix at the injector well is presented in Appendix A

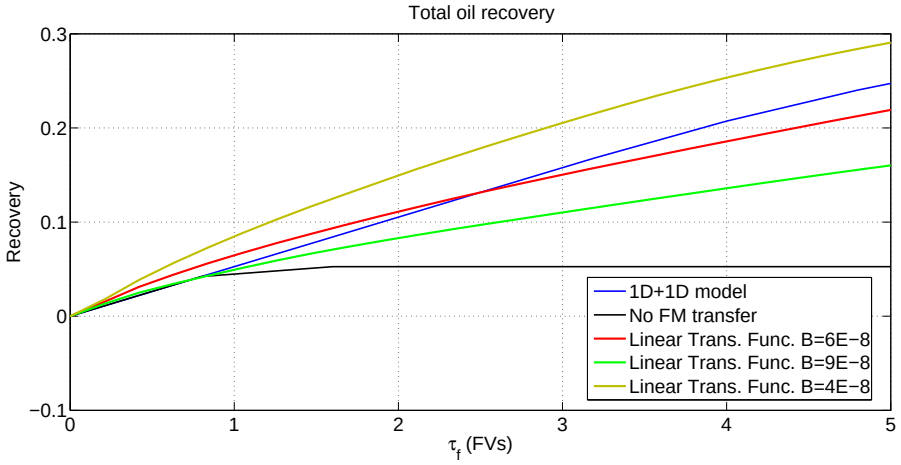


Figure 5.2: Oil recovery calculated with linear transfer function model before breakthrough in PWW system

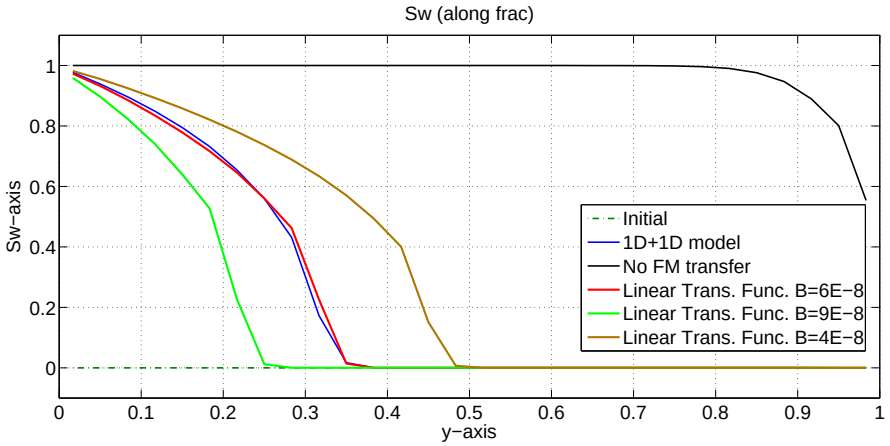


Figure 5.3: Water saturation along the fracture after injecting 1 FV comparison between the 1D+1D model and the linear transfer function model

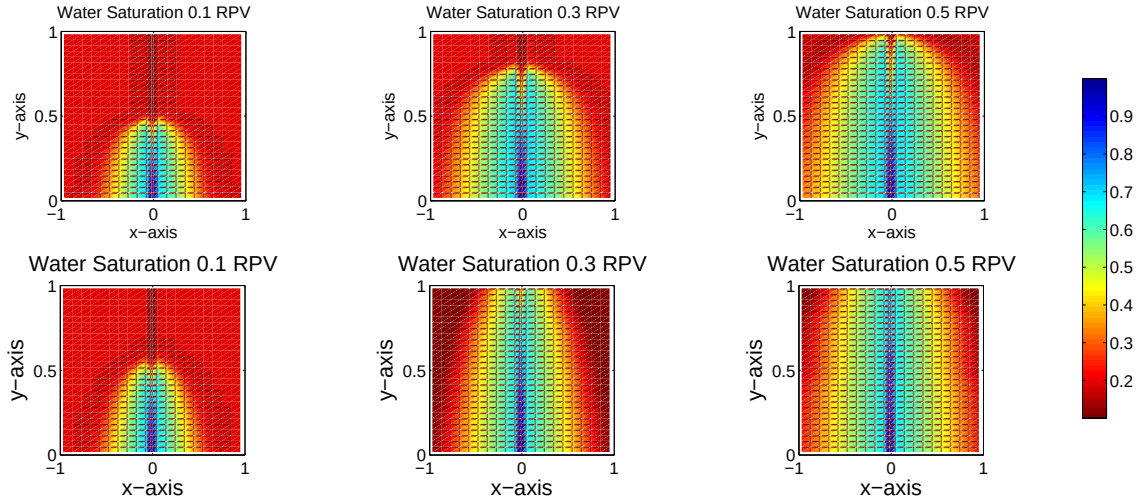


Figure 5.4: Calculated water saturation, top left:using $LTF$ model after injecting 0.1 RPV,top middle:using $LTF$ model after injecting 0.3 RPV, top right:using $LTF$ model after injecting 0.5 RPV, bottom left:using 1D+1D model after injecting 0.1 RPV, bottom middle:using 1D+1D model after injecting 0.3 RPV, bottom right:using $LTF$ model after injecting 0.5 RPV

## 5.2 Comparing the 1D+1D model to the linear transfer function model in POW system

In this section, the 1D+1D model described by Eq. 3.25 and Eq. 3.30 will be compared to the linear transfer function model described by Eq. 3.44 and Eq. 3.47. To make this comparison, all constants for the base case are used as given in Table 4.1. The saturation curves for the POW case are used. 10 grid cells are used along x-direction in the matrix and 30 grid cells are used along the fracture.

Fig. 5.5 shows the oil recovery calculated with the linear transfer function and the 1D+1D model, after injecting 1 RPV. Various values of rate constants $B$ have been used ($B = 3E-8$, $2E-8$ and $1E-9$). The recovery calculated with the linear transfer function when $B = 1E-9$ matches closely the recovery calculated with the 1D+1D model. However, at early time, the linear transfer function over predicts the recovery. Furthermore, the linear transfer function predicts very similar oil recovery after injecting 4 FV's. It is possible to see that for $B = 3E - 8$ and $B = 2E - 8$ the oil recovery is higher than for $B = 1E - 9$.

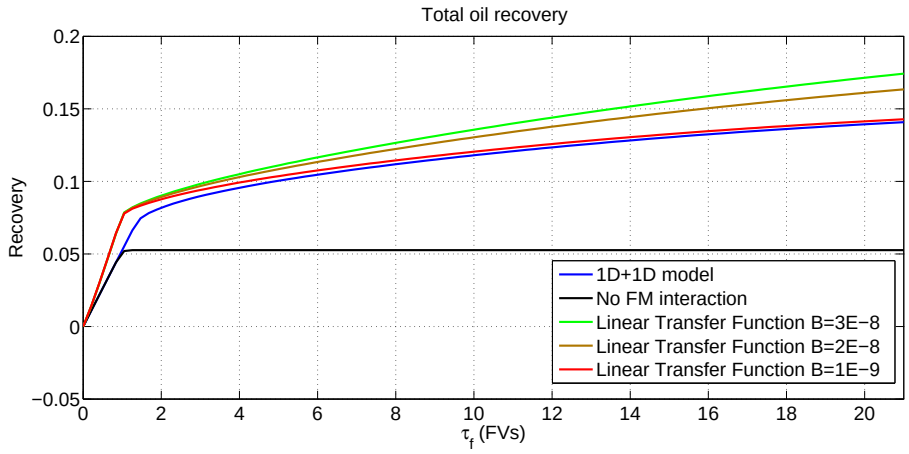


Figure 5.5: Oil recovery after injecting 1 RPV when using linear transfer function in POW system

Fig. 5.6 shows a comparison when 1 FV has been injected. For various values of rate constant $B$. The figure shows that there is no match between the linear transfer function and the 1D+1D model. The mismatch between both models means that the linear transfer function model while giving an appropriate approximation of the oil recovery, fails to reproduce the water front inside the fracture before breakthrough. When $B = 1E - 9$, the water front inside the matrix is similar as if there were no fracture matrix interaction.

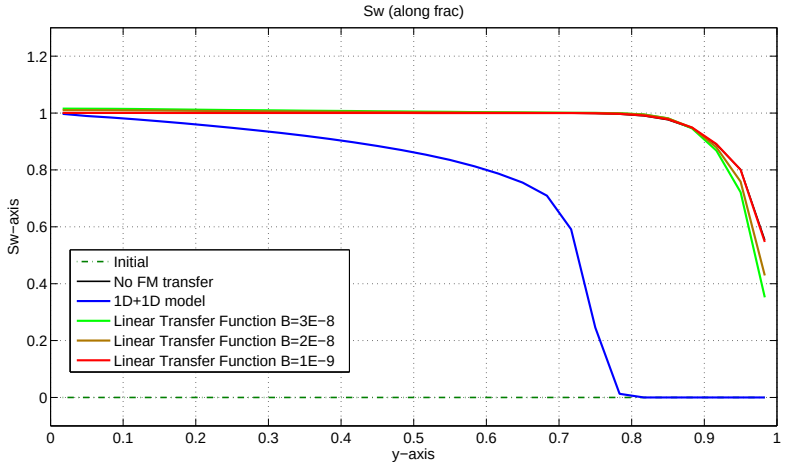


Figure 5.6: Water saturation along the fracture after injecting 1 FV comparison between the 1D+1D model and the linear transfer function in POW system

Additionally, the water saturation and capillary pressure in the matrix at the injector well is presented in Appendix B

## 5.3 The effect of grid size on rate constant $B$

In this section the effect of decreasing the grid size along the matrix and the fracture will be evaluated. Rate constant $B$ is expected to change to match the oil recovery calculated with the 1D+1D model. To make this comparison, all constants for the base case are used as given in Table 4.1. The saturation curves for the PWW and POW case are used. The grid cells along x-direction ($n_x$) and grid cells along the fracture ($n_y$) will be varied. The plots for oil recovery as a function of grid size are presented in Appendix C. These plots show that the rate constant $B$ is inversely proportional to the grid size. If the size of this cells is small the rate constant should increase.

## 5.4 The effect of matrix permeability $K^M$ on rate constant $B$

In this section the effect of changing the matrix permeability will be evaluated. To make this comparison, all constants for the base case are used as given in Table 4.1. The saturation curves for the PWW and POW case are used. 10 grid cells are used along x-direction in the matrix and 30 grid cells along the fracture. The matrix permeabilities used are $K^M = 1mD$, $5mD$ and $25mD$

Fig. 5.7 shows that when changing the matrix permeability, the rate constant $B$ should be adjusted to match oil recovery calculated with the 1D+1D model. When the matrix permeability increases, the rate constant $B$ decreases to match the oil recovery given by the 1D+1D model. It is seen that in PWW systems, the rate constant $B$ is directly proportional to the permeability.

Fig. 5.8 shows that when the matrix permeability increases, the rate constant $B$ increases to match the oil recovery given by the 1D+1D model. It is seen that in POW systems, the rate constant $B$ is directly proportional to the permeability.

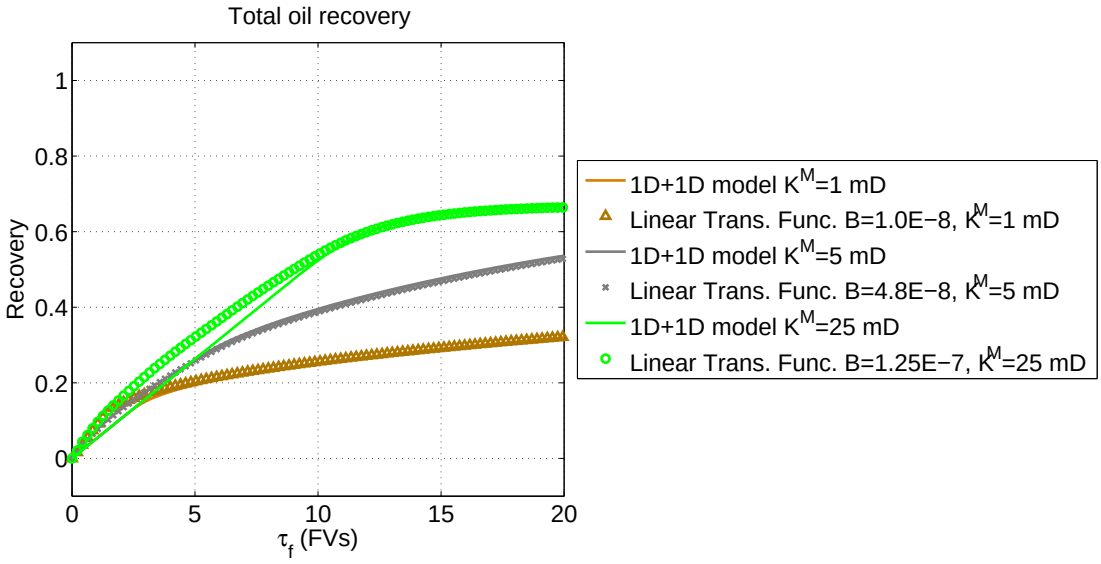


Figure 5.7: Oil recovery after injecting 1 RPV in PWW system calculated with the linear transfer function and the 1D+1D model for various values of matrix permeability $K^M$

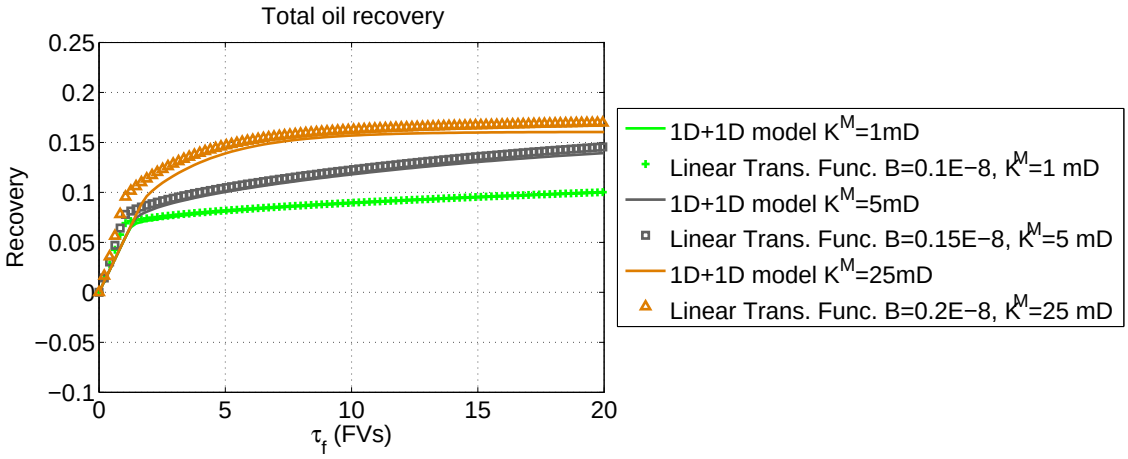


Figure 5.8: Oil recovery after injecting 1 RPV in POW system calculated with the linear transfer function and the 1D+1D model for various values of matrix permeability $K^M$

## 5.5 The effect of matrix porosity $\phi^M$ on rate constant $B$

In this section the effect of changing the matrix porosity will be evaluated. To make this comparison, all constants for the base case are used as given in Table 4.1. The saturation curves for the PWW and POW cases are used. 10 grid cells are used along x-direction in the matrix and 30 grid cells along y-direction in the fracture. The matrix porosities used are $\phi^M = 0.1$, 0.2 and 0.3

Fig.5.9 shows that when changing the matrix porosity, the rate constant $B$ should be adjusted to match the 1D+1D model oil recovery. It is noted that the rate constant $B$ is inversely proportional to matrix porosity in a PWW system. It is interesting to note that when matrix porosity is $\phi^M = 0.1$ the oil recovery is the highest compared to the other porosities evaluated. This is because imbibition is especially effective at low porosity.

If we recall the relations for parameters $\alpha$ (Eq. 3.28) and $\beta$ (Eq. 3.23), we can see that $\alpha$ is inversely proportional to matrix porosity and $\beta$ directly proportional to matrix porosity. Increasing matrix porosity will decrease $\alpha$ and increase $\beta$ hence reducing oil recovery. This scenario has been evaluated in Section 4.6, the result was shown in Fig. 4.15.

Fig.5.10 shows that the rate constant $B$ is inversely proportional to matrix porosity in a POW system. As discussed in the previous figure, at $\phi^M = 0.1$ the oil recovery is the highest compared to the other porosities evaluated.

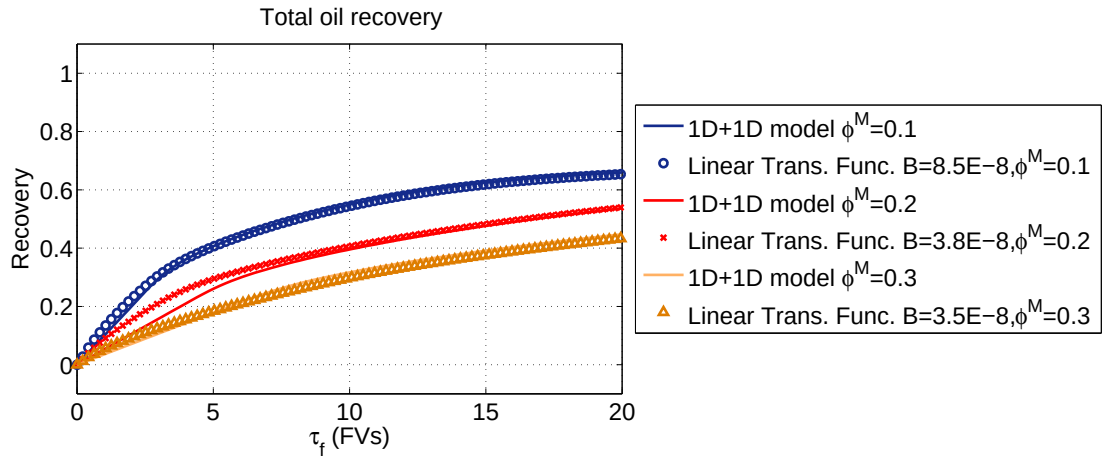


Figure 5.9: Oil recovery after injecting 1 RPV in PWW system calculated with the linear transfer function and the 1D+1D model for various values of matrix porosity $\phi^M$

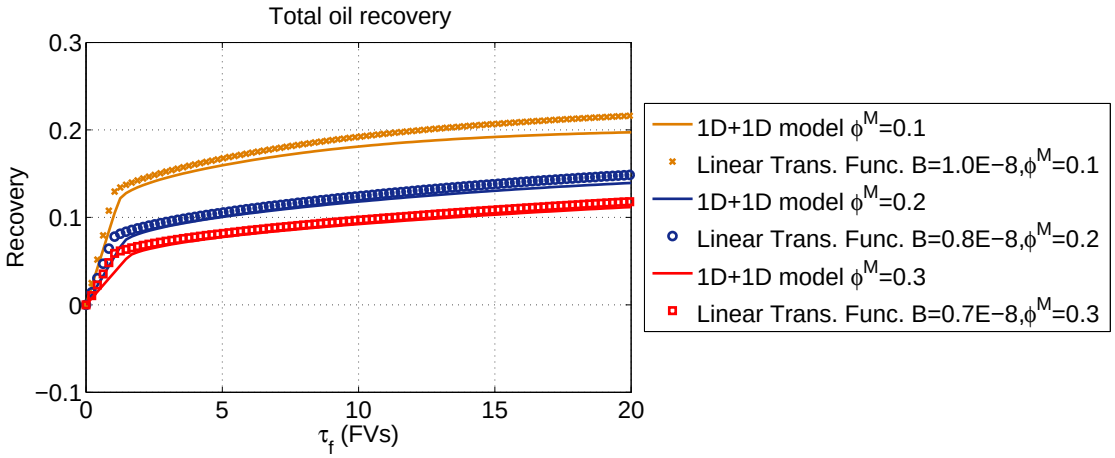


Figure 5.10: Oil recovery after injecting 1 RPV in POW rock calculated with the linear transfer function and the 1D+1D model for various values of matrix porosity $\phi^M$

# Chapter 6

# Discussion and conclusions

A discussion of the numerical investigations made during this work is presented and conclusions are drawn to answer the objectives posed on Section 1.3. The discussion is developed based on the results presented here and the information obtained from the literature review.

## 6.1 Discussion on the 1D+1D model

When using the 1D+1D model with different saturations curves, clear differences appear. The effect of the capillary pressure curve on oil recovery is very important, this was studied in Section 4.4. The concept of imbibition potential ($\Delta S = S_{eq} - S_0$) is very important. When the rock is POW the imbibition potential is $\Delta S^{mPOW} = 0.1$, when the rock is PWW the imbibition potential is $\Delta S^{mPWW} = 0.6$. This characteristic seems to dominate the amount of imbibition that will take place in fracture matrix flow. The higher the imbibition potential, the more imbibition will be. Fig. 4.7 shows the difference in oil recovery when the system is PWW compared to a POW system. In Section 3.3, the 1D+1D model was scaled and two dimensional numbers were obtained $\alpha$ and $\beta$. If we consider Eq.3.28 and Eq.3.23, it is noted that by varying the dimensional numbers $\alpha$ and $\beta$, the effect of 9 variables (Well spacing $L_y$, Fracture aperture $2b$, Fracture porosity $\phi^f$, Matrix porosity $\phi^m$, Matrix thickness $L_x$, Fracture pore velocity $v_T^f$, Matrix permeability $K^m$, Oil viscosity $\mu_o$ and Initial capillary pressure $P_{c,max}$.) is considered.

When studying the 1D+1D model in Section 4.5, the effect of changing $\alpha$ parameter was evaluated when keeping $\beta$ constant. From Eq. 3.23 it is possible to see that $\alpha$ is directly proportional to the well spacing $L_y$, matrix permeability $K^m$, initial capillary pressure $P_{c,max}$ and inversely proportional to fracture pore velocity $v_T^f$, matrix porosity $\phi^m$, matrix thickness $L_x$ and oil viscosity $\mu_o$.

When $\alpha$ is large, the water will imbibe deep in the matrix. More water is drawn

from the fracture into the matrix. Increasing $\alpha$ improves oil recovery as given by Fig. 4.12. It also generates a delay in the water front inside the fracture.

When $\alpha$ is small, the water will flow through the fracture, and only the nearest region of the matrix will imbibe water. This will reduce the total oil recovery and generate early water breakthrough.

When varying $\alpha$, it is possible to distinguish two flow regimes. When $\alpha$ is large the "filling fracture" and "instantly filled" regimes [20] can be identified. When $\alpha$ is small, only the "instantly filled" regime is observed on the oil recovery curve (Fig. 4.12 middle and right).

Reducing fracture pore velocity $v_T^f$ increases $\alpha$ which improves oil recovery. Hence, a lower injection rate represents a more efficient uptake of water by the matrix.

When studying the 1D+1D model in Section 4.6, the effect of changing $\beta$ parameter was evaluated in two scenarios, first when keeping $\alpha$ constant and then when changing $\alpha$. From Eq. 3.28 it is possible to see that $\beta$ is directly proportional to matrix thickness $L_x$, matrix porosity $\phi^m$, and inversely proportional to fracture aperture $2b$ and porosity $\phi^f$.

First the scenario when increasing $\beta$ at constant $\alpha$ is discussed. This can only be achieved by decreasing fracture aperture $2b$ or/and porosity $\phi^f$. However, it is important to keep in mind that in the 1D+1D model, if fracture aperture $2b$ is changed, so is the injection rate, as given by the following relationship $InjectionRate = 2bv_T^f$. When decreasing the fracture aperture $2b$, oil recovery will increase as depicted in Fig. 4.14, the reason for this increase is that the injection rate is reduced, this means that in order to inject a given volume, more time is required, giving more time for imbibition to occur.

The scenario when increasing $\beta$ and reducing $\alpha$ is discussed now. This scenario takes place when decreasing the fracture aperture $2b$ and increasing pore velocity $v_T^f$ to keep a constant injection rate. Increasing parameter $\beta$ and decreasing $\alpha$ increases oil recovery as depicted in Fig. 4.15. The highest oil recovery in this figure describes a scenario when the fracture is wide, and the water takes more time to travel in the fracture, hence there is more time for interaction with the matrix to occur. This is consistent with experiments presented in [20]. Where the fracture aperture was studied by using a computer tomography scanner to take images of the fluids saturations, in these studies the amount of spontaneous imbibition registered was directly proportional to the fracture width.

When varying $\beta$, it is possible to distinguish two flow regimes in the oil recovery curves in Fig. 4.14. When $\beta$ is large the "filling fracture" regime is dominant and the oil recovery is a linear function of time. When $\beta$ is small, two flow regimes are present, the "filling fracture" and "instantly filled" [20]. The oil recovery is a linear function of time before breakthrough and non-linear after it.

When studying the 1D+1D model in Section 4.7, the effect of changing the viscosity ratio ($M = \mu_w/\mu_o$) is evaluated. From Eq. 3.23 and Eq. 3.28 it is possible to see that changing $\mu_w$ can modify the viscosity ratio $M$ and keep $\alpha$ and $\beta$ constant.

Changing the viscosity ratio $M = \mu_w/\mu_o$ affects the fractions flow functions in matrix ($f_W^M$) and the fracture ($f_W^f$). as given by Fig. 4.16.

When the viscosity ratio is low ($\mu_w/\mu_o = 1/5$), the displacement of oil in the fracture is not as efficient as in the base case ($\mu_w/\mu_o = 1$). However, more water imbibes in the matrix in this case. This is because water flows more easily. Reducing the water viscosity will increase oil recovery by spontaneous imbibition.

When the viscosity ratio is high ($\mu_w/\mu_o = 5$), the displacement of oil in the fracture is more efficient compared to the base case ($\mu_w/\mu_o = 1$). The mobility of the water phase is reduced, decreasing the amount of oil produced by spontaneous imbibition.

## 6.2 Discussion on the linear transfer function

In Section 5, a comparison between the 1D+1D model (Eq. 3.25, Eq. 3.30) and the linear transfer function model (Eq. 3.44, Eq. 3.47) was made. The goal was to test the linear transfer function of the form $T = B\phi^M(S_{eq} - S^M)$ (see Section 2.2.1), where $B$ is a rate constant given in $1/s$.

The idea was to understand the physical properties that determine the rate constant $B$. The properties evaluated were rock wettability, effect of grid size, matrix permeability and porosity. After computing the oil recovery with the 1D+1D model for a given set of properties, the rate constant $B$ was adjusted to match as close as possible the 1D+1D oil recovery curve. Section 5.1 compares the 1D+1D model and the linear transfer function model for a PWW system. A value of $B = 6E-8$ matches the oil recovery curve of the 1D+1D model. The rate constant found is close to the value used in [7], where the linear transfer function was used to evaluate water flooding of a Chinese oil field, using a rate constant $B = 8E-8$ for a system between PWW and mixed-wet. The values of $B = 6E-8$, reproduces closely the water front in the fracture, the water saturation and capillary pressure in the matrix.

It is important to note that the linear transfer function model cannot reproduce the linear behaviour of the oil recovery curve before breakthrough. This is because the transfer function was derived under the assumption that the oil recovery curve is an exponential function of time. In Section 5.2, a POW system is considered. It was found that a value of $B = 1E-9$ matches the oil recovery curve of the 1D+1D model. However, this values fails to reproduce the water front in the fracture before breakthrough. From this observation it is inferred that the linear

transfer function fails to reproduce completely the physics of the fracture matrix flow before breakthrough.

In Section 5.3, the effect of grid size on the rate constant $B$ is studied. The saturation curves for the PWW case and the properties of Table 4.1 were used. It was found that the grid size plays a role modifying the rate constant (Table 6.1). If a small grid size is going to be used, the rate constant $B$ should increase to match the oil recovery calculated with the 1D+1D model.

Table 6.1: Rate constant $B$ as function of grid size

| Rate constant $B$ $1/s$ | grid cells along x-direction $n_x$ | grid cells along the y-direction $n_y$ |
|---|---|---|
| 6E-8 | 10 | 30 |
| 6E-8 | 20 | 60 |
| 9E-8 | 40 | 120 |

In Section 5.4, the effect of matrix permeability $K^M$ on rate constant $B$ is evaluated, it is found that $B$ is directly proportional to the matrix permeability, that is $B \propto K^M$.

In Section 5.5, the influence of matrix porosity $\phi^M$ on rate constant $B$ is evaluated. It is noticed that $B$ is inversely proportional to the matrix porosity, that is $B \propto \frac{1}{\phi^M}$

It is relevant to compare the findings about the rate constant $B$, with the relation found in the literature to calculate this parameter $B = b\sqrt{\frac{K^M}{\phi^M}}\frac{\sigma}{L_c^2\sqrt{\mu_o\mu_w}}$ (Eq. 2.6).

The relations found in the literature shows good agreement with the findings from the linear transfer function testing since they show that $B$ is directly proportional to matrix permeability and inversely proportional to matrix porosity.

It is noted that the oil-water interfacial tension is part of the relation. However, since the 1D+1D model does not consider interfacial tension, it was not possible to test the influence of this property.

## 6.3 Conclusions

The main objective of this work is to understand the factors affecting spontaneous imbibition by the use of a 1D+1D model.

The following conclusions are drawn based on the objectives stated in Section 1.3.

1. The role of saturation curves was studied qualitatively, showing that the wettability of the system is the driving factor influencing oil production by

spontaneous imbibition. When waterflooding takes place, a preferentially water-wet system produces significantly more oil than a preferentially oil wet system.

2. Respect to the dimensionless parameters $\alpha$ and $\beta$. When $\alpha$ increases at constant $\beta$, the water imbibes deep in the matrix. Increasing $\alpha$ improves oil recovery. When $\alpha$ is small, only the "instantly filled" regime is observed on the oil recovery curve, generating poor oil recovery.

   When increasing $\beta$ at constant $\alpha$, oil recovery will increase, this is because water injection rate is reduced.

   Increasing parameter $\beta$ and decreasing $\alpha$ increases oil recovery. This describes an scenario when the fracture is wide, and the water takes more time to travel in the fracture, hence there is more time for imbibition to occur.

   When $\beta$ is large the "filling fracture" regime is dominant and the oil recovery is a linear function of time. When $\beta$ is small, two flow regimes are present, the "filling fracture" and "instantly filled".

3. When the viscosity ratio is low ($\mu_w/\mu_o = 1/5$), more water imbibes in the matrix compared to the base case ($\mu_w/\mu_o = 1$). This is because water flows more easily. Reducing the water viscosity increases oil recovery by spontaneous imbibition.

   When the viscosity ratio is high ($\mu_w/\mu_o = 5$), the mobility of the water phase is reduced, decreasing the amount of oil produced by spontaneous imbibition.

4. The linear transfer function of the form $T = B\phi^M(S_{eq} - S_w^M)$ can reproduce the oil recovery curve produced with the original 1D+1D model. However, this transfer function cannot reproduce the linear recovery curve before breakthrough. This is because the linear transfer function was derived considering that oil recovery is an exponential function of time.

   The following relation was observed for the rate constant $B \propto \frac{K^M}{\phi^M}$. Where $K^M$ is the matrix absolute permeability and $\phi^M$ is the porosity.

# Bibliography


[1] W.G. Anderson. Wettability literature survey-part 4: Effects of wettability on capillary pressure. *Journal of Pretroleum Technology*, pages 1283–1300, 1987.

[2] W.G. Anderson. Wettability literature survey-part 5: The effects of wettability on relative permeability. *Journal of Pretroleum Technology*, pages 1283–1300, 1987.

[3] Zheltov Iu.P. Barenblatt G.I. and Kochina I.N. Basic concepts in the theory of seepage of homegeneous liquids in fissured rocks. *Journal of Applied Mathematical Mechanics*, 1960.

[4] A. Chatenever. Microscopic behavior of fluids in porous systems-final report on research project 47b. *Reseach and Occurrence of Petroleum API*, pages 69–80, 1955.

[5] F.F. Craig. The reservoir engineering aspects of waterflooding. *SPE*, Monograph Series, 1941.

[6] Blunt M. Di Donato G., Huang W. Streamline-based dual porosity simulation of fractured reservoirs. *SPE Annual Technical Conference*, 2003.

[7] Tavassoli Z. Blunt M. Di Donato G., Lu H. Multirate-transfer dual-porosity modeling of gravity drainage and imbibition. *SPE Journal*, 2007.

[8] Norwegian Petroleum Diroctorate. Facts 2013 - the norwegian petroleum sector. *The Ministry of Petroleum and Energy and the Norwegian Petroleum Directorate*, 2013:71, 2013.

[9] E.C.Donalson and R.D.Thomas. Microscopic observations of oil displacement in water-wet and oil-wet systems. *SPE*, 1971.

[10] M.Blunt E.Unsal, S.Matthai. Simulation of multiphase flow in fractured reservoirs using a fracture-only model with transfer functions. *Comput Geosci*, 2008.

[11] Nnaemeka Ezekwe. Petroleum reservoir engineering practice. *Prentice Hall*, 2010.

[12] S. Geiger. A novel multirate dual-porosity model for improved simulation of fractured and multiporosity reservoirs. *SPE Journal*, 2013.

[13] Kazemi H. Gilman J.R. Improvement in simulation of naturally fractured reservoirs. *SPEJ*, (23):695–707, 1983.

[14] H.Y.Jennings. Surface properties of natural and syntetic porous media. *Prod Monthly*, 21(5):20–24, 1957.

[15] H. Kazemi. Numerical simulation of water-oil flow in naturally fractured reservoirs. *SPE-AIME*, Transactions, 1976.

[16] M.C. Leverett. Capillary behaviour in porous media. *Trans AIME*, 142:152–169, 1941.

[17] Mason G. Morrow M. Recorevy of oil by spontaneous imbibition. *Current Opinion in Colloid and Interface Science*, (6):321–337, 2001.

[18] G. Mason M.R.Morrow. Recovery of oil by spontaneous imbibition. *Colloid Interdace Sci*, 6:321–337, 2001.

[19] P.Andersen. A model for spontaneous imbibition as a mechanism for oil recovery in fractured reservoirs. *Transp Porous Med*, 2013.

[20] Kovscek A.R. Rangel-German E.R. Experimental and analytical study of multidimensional imbibition in fractured porous media. *U.S. Department of Energy*, 2002.

[21] A.M. Saidi. Simulation of naturally fractured reservoirs. *SPE Journal*, Symposium on Reservoir Simulation:16–18, 1983.

[22] Pallav Sarma. New transfer functions for simulation of naturally fractured reservoirs with dual porosity models. *Department of Petroleum Engineering of Standford University*, 2003.

[23] Schlumberger. Eclipse technical description-dual porosity. pages 235–270, 2010.

[24] L.E.Treiber S.H.Raza and D.L.Archer. Wettability of reservoir rocks and its evaluation. *Prod Monthly*, 32(4):2–7, 1968.

[25] Owens Treiber, Archer. A laboratory evaluation of the wettability of fifty oil-producing reservoirs. *SPE Journal*, pages 531–540, 1972.

[26] Morrow N.R.and Ma S. Zhang X. Experimental verification of a modified scaling group for spontaneous imbibition. *SPERE11*, SPE-30762-PA:280–285, 1996.

# Appendix A

# Matrix saturation and capillary pressure plots for Preferentially Water-Wet system

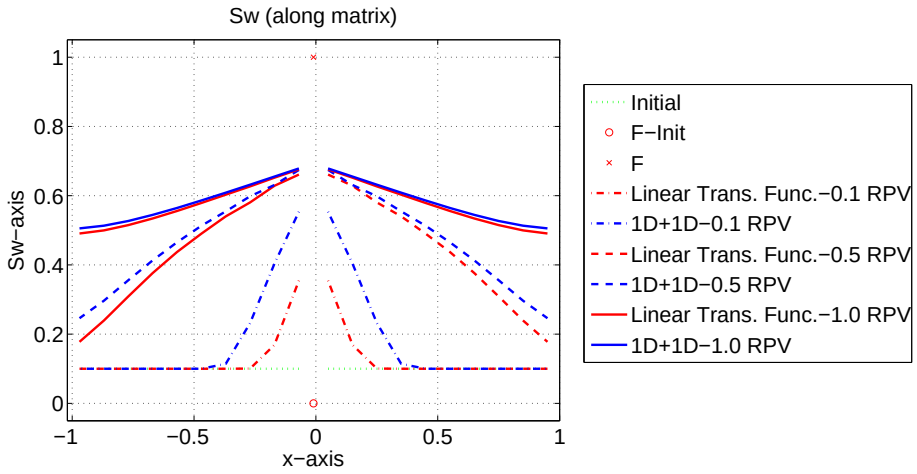


Figure A.1: Water saturation along the matrix

Fig. A.1 presents the water saturation along the matrix at the injector well for different injected volumes for a PWW system. After injecting 0.1 RPV, the linear transfer function shows slower advance of the water front inside the matrix compared to the 1D+1D model. The gap is considerable, but this gap reduces when the injected volume is 0.5 RPV. When 1.0 RPV has been injected, the water front inside the matrix for the linear transfer function and the 1D+1D model is

similar.

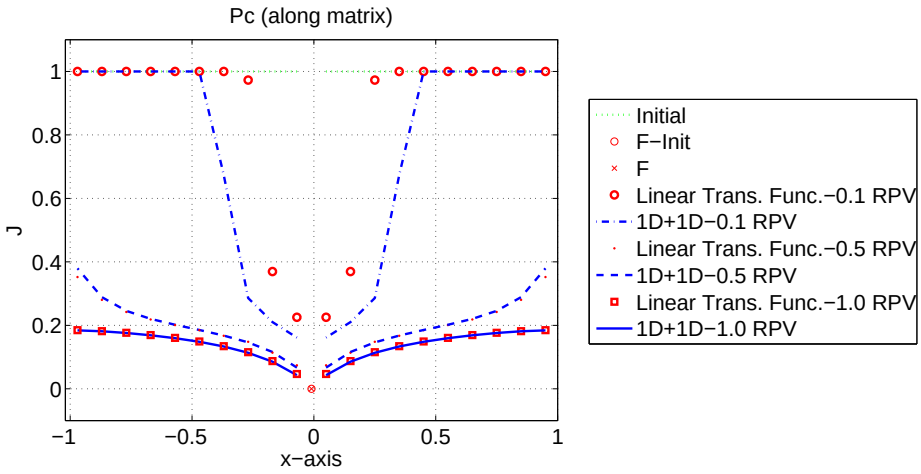


Figure A.2: Capillary pressure along the matrix

Fig. A.2 presents the capillary pressure along the matrix at the injector well for different injected volumes for a PWW system. The capillary pressure inside the matrix calculated with the linear transfer function model when 0.1 RPV has been injected is lower than the capillary pressure calculated with the 1D+1D model. However, when 1.0 RPV has been injected, the capillary pressure inside the matrix is similar for both models.

# Appendix B

# Matrix saturation and capillary pressure plots for Preferentially Oil-Wet system

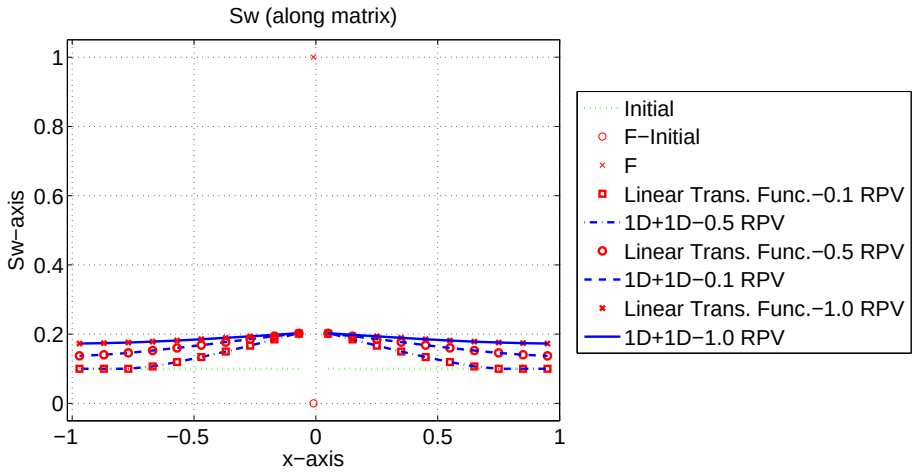


Figure B.1: Water saturation along matrix for various injected volumes in POW rock calculated with the linear transfer function and the 1D+1D model

Fig. B.1 presents the water saturation along the matrix at the injector well for different injected volumes for a POW system. Since the rock is POW the water saturation along the matrix remains bellow 0.2. Low imbibition is observed as

expected for the POW rock. The constant $B = 1E-9$ was used. A perfect match between the linear transfer function and the 1D+1D model is distinguished.

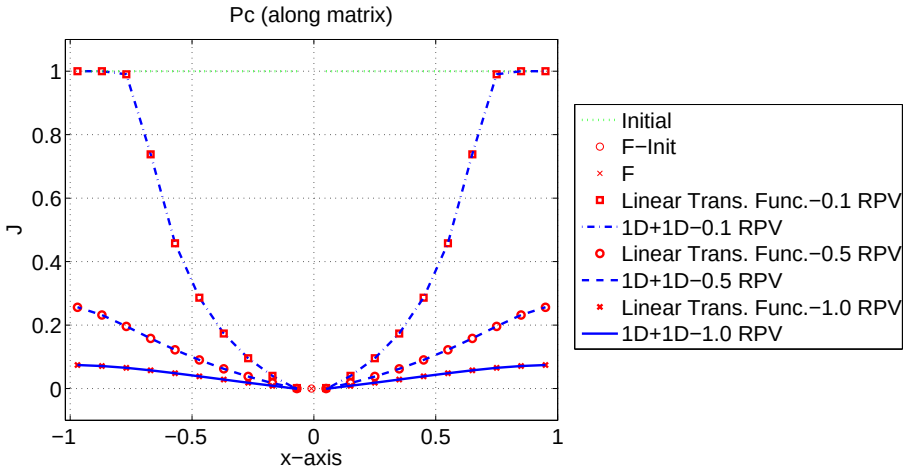


Figure B.2: Capillary pressure along matrix for various injected volumes in POW rock calculated with the linear transfer function and the 1D+1D model

Fig. B.2 presents the capillary pressure along the matrix at the injector well for different injected volumes for a POW system. The constant $B = 1E-9$ was used. Capillary pressure reduces as injected volume increases. A perfect match between the linear transfer function and the 1D+1D model is distinguished.

# Appendix C

# Influence of grid size on rate constant $B$

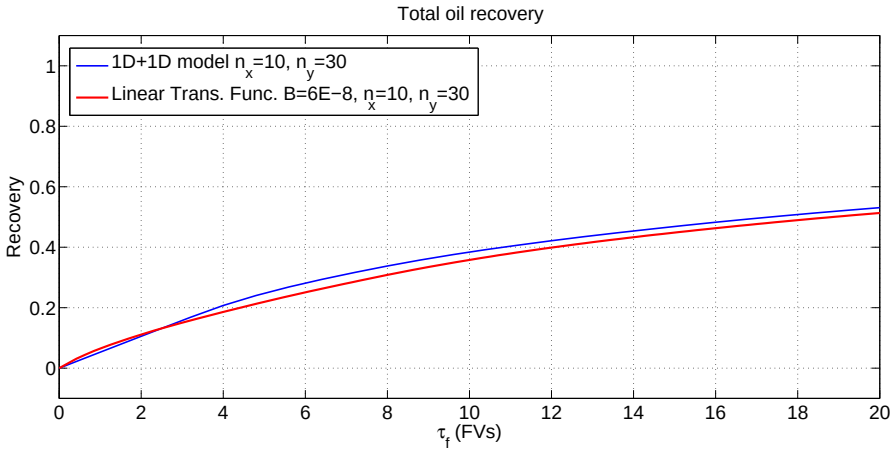


Figure C.1: Oil recovery after injecting 1 RPV in PWW system calculated with the linear transfer function and the 1D+1D model with $n_x = 10$ and $n_y = 30$

Fig. C.1 shows the oil recovery calculated with the 1D+1D model and the linear transfer function when rate constant $B = 6E - 8$ and the grid size is given by $n_x = 10$ and $n_y = 30$. As discussed previously, there is a close match, meaning that the rate constant $B$ is appropriate.

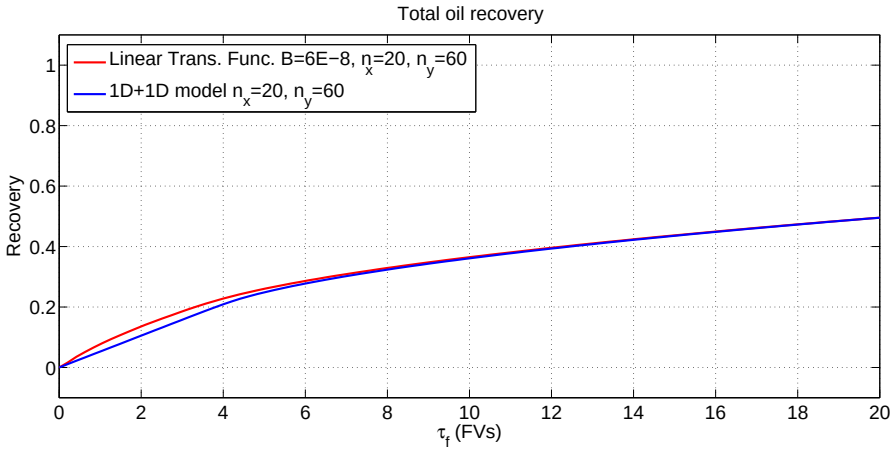


Figure C.2: Oil recovery after injecting 1 RPV in PWW system calculated with the linear transfer function and the 1D+1D model with $n_x = 20$ and $n_y = 60$

Fig. C.2 shows the oil recovery calculated with the 1D+1D model and the linear transfer function when rate constant $B = 6E - 8$ and the grid size is given by $n_x = 20$ and $n_y = 60$. As discussed previously, there is a close match, meaning that the rate constant $B$ is still appropriate.

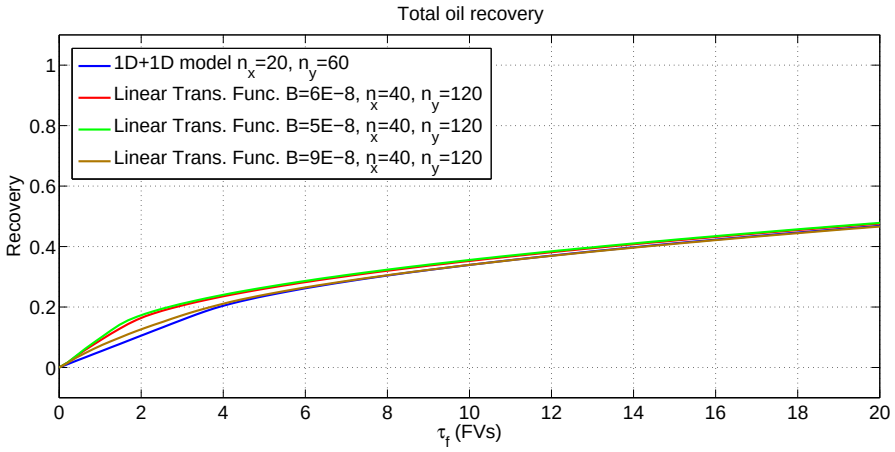


Figure C.3: Oil recovery after injecting 1 RPV in PWW system calculated with the linear transfer function and the 1D+1D model with $n_x = 40$ and $n_y = 120$

Fig. C.3 shows the oil recovery calculated with the 1D+1D model and the linear transfer function when rate constant $B = 5E-8$, $6E-8$, $9E-8$ and the grid size is given by $n_x = 40$ and $n_y = 120$. In this case, the rate constant $B = 6E-8$ is no longer appropriate to match the oil recovery from the 1D+1D model, instead $B = 9E-8$ gives a better match. This means that the rate constant is inversely proportional to the grid size.

# Appendix D

# Numerical discretization of the linear transfer function model

The discretization of the linear transfer function model is presented is this section. The discretization is similar to the one of the 1D+1D model presented in [19]. The governing equations described by Eq. 3.47 and Eq. 3.44 are solved using an operator splitting approach, where the scaled linear transfer function model is split in to the following two subsystems:

- **System 1: Flow in the y-direction**

$$\begin{aligned} \partial_t(S) &= 0 && (0 < x < 0; 0 < y < 1) \\ \partial_t(S) &= -\partial_y f_w^f && (-2/\beta < x < 0; 0 < y < 1) \end{aligned} \tag{D.1}$$

- **System 2: Flow in the x-direction**

$$\begin{aligned} \partial_t(S) &= -\alpha\partial_x(\frac{\lambda_o^M f_w^M}{D_{av}^M}\partial_x J^m) && (0 < x < 0; 0 < y < 1) \\ \partial_t(S) &= -\alpha(\frac{\phi^M L_x^2 \mu_o}{\phi^f b K^M P_{max}})B\phi^M(S_{eq}^M - S_w^M) && (-2/\beta < x < 0; 0 < y < 1) \end{aligned} \tag{D.2}$$

Discretization of System 1 is presented in [19] and will not be discussed here. The discretization of System 2 is discussed now, even though the discretization is similar to the one presented in [19], the interaction between the matrix and fracture now is represented by the transfer function. This system is convenient to consider relatively to the dimensionless time $t^* = \frac{t}{\tau^M}$. Consequently, the model of

Eq. D.2 takes the form (where we skip the $*$ superscript).

$$\begin{aligned}
\partial_t(S) &= -\partial_x(\frac{\lambda_o^M f_w^M}{D_{av}^M}\partial_x J^m) \qquad\qquad (0<x<0; 0<y<1) \\
\partial_t(S) &= -(\frac{\phi^M L_x^2 \mu_o}{\phi^f b K^M P_{max}})B\phi^M(S_{eq}^M - S_w^M) \quad (-2/\beta<x<0; 0<y<1)
\end{aligned} \tag{D.3}$$

The fracture is connected to the matrix by letting the fracture be cell 1 in the grid and the cells 2 to ,...,$N_x+1$ cover the $N_x$ cells of the matrix.

To describe the flow in the interior part of the matrix the first equation of Eq.D.3 is used:

$$\frac{S_i^{n+1}-S_i^n}{\Delta t} = -\frac{(\lambda_o^M f_w^M)_{i+1/2}\frac{J_{i+1}^M - J_i^M}{\Delta x} - (\lambda_o^M f_w^M)_{i-1/2}\frac{J_i^M - J_{i-1}^M}{\Delta x}}{\Delta x} \quad (i=3,..,N_x) \tag{D.4}$$

The coefficients $(\lambda_o^M f_w^M)_{i+1/2}$ are evaluated as described in [19].

At the first cell in the matrix region we have:

$$\frac{S_2^{n+1}-S_2^n}{\Delta t} = -\frac{(\lambda_o^M f_w^M)_{2+1/2}\frac{J_3^M - J_2^M}{\Delta x} - (\lambda_o^M f_w^M)_{2-1/2}\frac{J_2^M - J_1^f}{\Delta x/2}}{\Delta x} \qquad (i=2) \tag{D.5}$$

At the last cell we have:

$$\frac{S_{N_x+1}^{n+1}-S_{N_x+1}^n}{\Delta t} = -\frac{-(\lambda_o^M f_w^M)_{N_x+1/2}\frac{J_{N_x+1}^M - J_{N_x}^f}{\Delta x}}{\Delta x} \qquad (i=N_x+1) \tag{D.6}$$

At the fracture, the second equation of Eq. D.3 is used, then at the fracture cell we have:

$$\frac{S_1^{n+1}-S_1^n}{\Delta t} = -(\frac{\phi^M L_x^2 \mu_o}{\phi^f b K^M P_{max}})B\phi^M(S_{eq}^M - S_2^n) \qquad (i=1) \tag{D.7}$$

# Appendix E

# Nomenclature

Table E.1: Variables

| **Variables** | **Name** | **Units** |
|---|---|---|
| $L_y$ | Well spacing | m |
| $L_x$ | Matrix thickness | m |
| $b$ | Half fracture aperture | m |
| $\phi^f$ | Fracture porosity | - |
| $\phi^m$ | Matrix porosity | - |
| $v_T^f$ | Fracture pore velocity | m/d |
| $K^m$ | Matrix permeability | mD |
| $\mu_o$ | Oil viscosity | cp |
| $\mu_w$ | Water viscosity | cp |
| $P_{c,max}$ | Initial capillary pressure | pa |
| $V$ | Pore volume | $m^3$ |
| $\tau$ | Time for flow | s |
| $T$ | Mass transfer rate | 1/s |
| $B$ | Mass transfer rate constant | 1/s |
| $\alpha$ | Ratio of time for flow in the fracture to time for capillary flow in the matrix | - |
| $\beta$ | Ratio of matrix pore volume to fracture pore volume | - |
| $\gamma$ | Ratio of time for flow in the fracture to time for capillary flow in the fracture | - |
| $J$ | J Leverett function | - |
| $S$ | Saturation | - |
| $\lambda$ | Phase mobility | mD/cp |
| $p$ | phase pressure | pa |

*Continued on next page*

Table E.1 – *Continued from previous page*

| **Variables** | **Name** | **Units** |
|---|---|---|
| $f$ | fractional flow function | - |
| $g$ | gravity $m/s^2$ | |
| $z$ | vector pointing downwards | - |
| $\Omega$ | Fracture/Matrix domain | - |
| $\Gamma$ | Injection/Production domain | - |
| $x$ | Length x-direction | m |
| $y$ | Length y-direction | m |
| $t$ | Time | s |
| $D$ | Dimensionless scaled capillary diffusion coefficient | - |
| $a_1$ | Parameter of the J function | - |
| $a_2$ | Parameter of the J function | - |
| $b_1$ | Parameter of the J function | - |
| $k_1$ | Parameter of the J function | - |
| $k_2$ | Parameter of the J function | - |
| $\Delta S$ | Imbibition potential | - |
| $M$ | Water-oil viscosity ratio | - |

Table E.2: Abbreviations

| | |
|---|---|
| DFDM | discrete fracture discrete matrix |
| FV | Fracture volume |
| LTF | Linear transfer function |
| NFR | Naturally fractured reservoir |
| SCDC | Scaled capillary diffusion coefficient |
| POW | Preferentially oil-wet |
| PWW | Preferentially water-wet |
| RPV | Reservoir pore volume |

Table E.3: Subscripts

| **Variables** | **Name** |
|---|---|
| $av$ | Average |
| $eq$ | Equilibrium |
| $c$ | Capillary |
| $o$ | Oil phase |
| $w$ | Water phase |
| $max$ | Maximum |
| 0 | Initial |
| $t$ | Total |
| $r$ | Relative |
| $x$ | Along x-direction |
| $y$ | Along y-direction |

Table E.4: Supercripts

| **Variables** | **Name** |
|---|---|
| $c, f$ | Capillary flow in fracture |
| $c, M$ | Capillary flow in matrix |
| $f$ | Fracture |
| $n$ | Time level |
| $M$ | Matrix |
| $'$ | Dimensionless |
| $*$ | Normalized |